Innovative Platform Design for In Vitro Primary Blast Injury Research

Noah Wade Showalter

Thesis submitted to the faculty of the Virginia Polytechnic Institute and State University
in partial fulfillment of the requirements for the degree of

Master of Science
In
Biomedical Engineering

Pamela J. VandeVord, Chair
Eric Jacques
Bhuvana Srinivasan

April 24th, 2023
Blacksburg, Virginia

Keywords: Electrical Explosion of Wire, Shock Wave, Primary Blast Injury

Innovative Platform Design for In Vitro Primary Blast Injury Research

Noah Wade Showalter

ABSTRACT

One of the principal challenges of primary blast injury research is imitation of shock waves accurately and consistently in a safe and tunable platform. Existing simulators have been effective in these goals but have not been conducive for *in vitro* models due to their large size and air-mediated wave propagation.

In this thesis, a redesigned benchtop shock wave generator (SWG) has provided a platform for *in vitro* models. A pulsed power generator charges a capacitor and discharges the capacitor through a bridge wire. The discharge causes the bridge wire to experience phase changes, momentarily becoming a gas or plasma. In this moment, the bridge wire expands radially and creates a pressure wave in the surrounding water. As the wave propagates, it forms a shock wave and strikes the cell platform at the far end of the conical tank. Current design efforts are focused on the tunability of the SWG, by varying the bridge wire material and diameter.

Five materials at three bridge wire diameters have been tested. Each bridge wire was inserted into the SWG via a pinching mechanism. Either side of the pinching mechanism was connected to either terminal of the capacitor. When the pulsed power generator was cycled, the bridge wire was vaporized and generated a shock wave. A piezoelectric sensor near the wide end of the tank recorded the passing of the shock wave, which was used to derive various pressure metrics that correlate to injury. The sample size for each combination of diameter and material was five, with a grand total of seventy-five samples run.

Two-way ANOVAs measuring the impacts of bridge wire material and diameter on a variety of shock wave metrics found that the diameter played a significant role in determining the peak

overpressure and positive impulse generated while the main effect of material played a much smaller role. The interaction between material and diameter was also found to be significant.

The tunable benchtop SWG provides a platform for exploration of primary blast injury using *in vitro* models. By adjusting the bridge wire diameter, the SWG can generate waves with a variety of shock wave metrics, providing an opportunity for researchers to address various degrees of injury. With the addition of this technology to the efforts to understand primary blast injury, development of treatments and protective equipment can be expedited.

Innovative Platform Design for In Vitro Primary Blast Injury Research

Noah Wade Showalter

GENERAL AUDIENCE ABSTRACT

Primary blast injury, the injury caused by the blast wave moving through the body, has been affecting those exposed to blast for nearly a century, since the regular use of conventional explosives in World War I. As equipment and war has changed in the past two decades, there has been heightened interest in understanding the effects of blast waves on the body. To assist in this research, blast wave simulators have been developed to recreate the blast wave in a controlled environment. However, current designs are not conducive to experiments on cultured cells.

A new blast wave simulator, called the shock wave generator (SWG), has been designed as a platform for cultured cell-based experiments. The simulator generates a shock wave by exploding a thin bridge wire using high electrical current. The explosion occurs underwater, generating a shock wave capable of injuring cells at the opposite end of the tank.

A platform such as this provides multiple opportunities to tune the pressure metrics related to the shock waves. Bridge wire material and volume play critical roles in the resulting shock wave, working together to define the amount of energy required to vaporize the bridge wire. Five materials and three diameters, a derivative of the wire volume, were investigated to determine their impacts on the resulting peak pressure, positive duration, and positive impulse.

While wire material was not found to have a significant impact on peak pressure, wire diameter had a significant effect on the resulting overpressures. The thickest wire generated the lowest peak pressure while the thinner wires generated higher peak pressures. The thinner wires were not significantly different from one another. A similar result was found for positive duration and impulse.

Overall, the use of an exploding wire to generate shock waves is applicable as an injury mechanism for cell cultures in primary blast injury research. This work along with future work will provide a tunable and controlled platform that has opened a new frontier for investigating the primary blast injury.

ACKNOWLEDGEMENTS

I would like to thank my parents for the endless support they have provided over the course of my life up to this day. The loving and thought-provoking environment they cultivated as I grew up encouraged me to stay curious, demanded that I think critically, and challenged me to overcome obstacles. My sister has also been a great inspiration to me. She has an unending willingness to try new things, which has constantly encouraged me to try new things and further fed my curiosity.

I joined the Traumatic Nerve Technologies lab as a sophomore and quickly took on responsibilities related to the SWG. I cannot thank Dr. VandeVord enough for the opportunity she has provided me with and the trust she afforded a then-undergraduate and continues to afford me today. Further, I am so appreciative of her time in effort in both overseeing my development in the lab and for chairing my thesis committee. I also want to thank Brendan Arnold, Dr. Fernanda Guilhaume Correa, Kelsey Wilson, and Ryosuke Yokosawa for their never-ending patience and support as the SWG was remodeled. Further, they were always willing to help me perform my studies, spending hours on end loading a wire, blowing it up, and repeating the process.

Thank you to my committee members, Dr. Eric Jacques and Dr. Bhuvana Srinivasan. I got the opportunity to work with Dr. Jacques at his facility, a wonderful insight into the various applications of ABSs. I was also provided with the opportunity to learn about Dr. Srinivasan's work on plasma science, a wonderful insight into her world. I am so thankful for the constructive and thoughtful feedback they have both provided me as committee members.

I would like to acknowledge colleagues that I consider to be technical mentors. Carly Norris and Alli Nelson have been fantastic sources of technical knowledge within the lab, particularly in the instrumentation of the SWG and the development of the analysis scripts. Carly Norris was the go to person for understanding relevance of the shock wave to injury and the biomechanics involved. Much of the scripts I developed were heavily influenced by Alli Nelson's previously written

scripts. For aid in the design, implementation, and analysis of the PPG, I must thank Dr. Max Bareiss and Dan Weber. Their expertise fast tracked much of my learning in a previously unfamiliar field and was invaluable in the redesign of the circuit.

Lastly, I'd like to thank Mingang Kim and Parul Patil, two fantastic collaborators from the Statistical Applications and Innovations Group (SAIG) at Virginia Tech. Their input has ensured that the statistical approaches taken in this thesis were appropriate and that the conclusions drawn from this work were sound. I cannot thank them enough for their patience, expertise, and aid throughout this project.

TABLE OF CONTENTS

TABLE OF FIGURES

TABLE OF TABLES

LIST OF ABBREVIATIONS

Abbreviations	Expansion
ABS	Advanced Blast Simulator
ANOVA	Analysis of Variance
AWG	American Wire Gauge
bTBI	Blast-induced Traumatic Brain Injury
DAQ	Data Acquisition System
EEW	Electrical Explosion of Wire
HSD	Honestly Significant Difference
HV	High Voltage
HVPS	High Voltage Power Supply
ms	Millisecond
PPG	Pulsed Power Generator
psi	Pounds per Square Inch
SPDT	Single-Pole, Double-Throw
SW	Shock Wave
SWG	Shock Wave Generator
TBI	Traumatic Brain Injury
TKPMC	Tukey-Kramer HSD Paired Means Comparison
UEWE	Underwater Electrical Wire Explosion
U.S.	United States of America

1 INTRODUCTION

The exposure of servicemembers to blast waves has increased over the past century and overtaken gunshot wounds as the most common mechanism of injury on the battlefield [1], [2]. Explosives accounted for over 95% all traumatic brain injury (TBI) cases in Operation Iraqi Freedom, most often in the form of an improvised explosive devices [3]. In addition, servicemembers, including breachers and artillery operators, may also be regularly exposed to low-level blast waves through their own tactics and equipment, termed occupational blasts [4], [5].

Terrorist attacks such as the Oklahoma City Bombing in April 1995 [6], Madrid Train Bombings in March 2004 [7], Boston Marathon Bombing in April 2013 [8], and Brussels Bombing in March 2016 have exposed civilian populations to blast waves in quantities not seen before. Between 2000 and 2020, there has been an estimated 503,352 casualties from explosives used in terrorist attacks worldwide [9].

These exposures lead to various types of blast injuries, which are often categorized into five classes, each class distinguished by a unique aspect of the explosion [10]–[12]. After an explosive is detonated, an individual will first experience primary blast trauma. On the order of milliseconds, the blast wave passes through the body rapidly compressing and expanding the tissue. Secondary and tertiary trauma occurs as debris strikes the individual and the individual is thrown into other objects, respectively. Figure 1 visualized the primary, secondary, and tertiary blast injuries. Lastly, quaternary blast trauma, such as burns and inhalation injuries from fires and toxic fumes, are injuries caused by the resulting environment.

Figure 1. The types of injuries caused by an explosive. [13]

Of the four classes, primary blast injury has historically seen the least attention, due to the invisible nature of both the mechanism and injuries. Nonetheless, the abrupt and dramatic change in pressure followed by the oscillating pressure that compresses and expands tissue has been shown to trigger stress and injury responses throughout the body [7], [14], [15]. Many of these responses transition into chronic conditions that can dramatically deteriorate the quality of life for survivors [16]–[20]. From 2000 to 2019, over 97% of the $902.1 million awarded to blast-injury research worldwide was provided by the United States [21]. The United States (U.S.) Department of Defense, U.S. National Institute of Health and the U.S. Department of Veteran's Affairs have all provided funding with goals that include the development of better personal protective equipment and treatment strategies for those previously exposed.

One of the principal challenges of conducting research into primary blast trauma is consistent generation of realistic blast waves in a safe and tunable platform. Existing Advanced Blast Simulators (ABS) have been effective in meeting these demands and critical in progressing the field, providing a large-scale platform for animal, cadaver, and surrogate models [17], [22]–[25]. However, due to their

large size and air-mediated wave propagation, ABS' application is not practical for *in vitro* studies, studies based on cultured cells.

The VandeVord lab has been investigating the application of electrical explosion of wires (EEW) to generate a consistent and controlled shock wave (SW) in water [18], [26]. When high current is introduced to thin, bare bridge wire, the material comprising the wire rapidly changes states of matter until finally forming a gas or plasma channel. The rapid expansion of this metal channel transfers the electrical energy into the surrounding medium as an SW, along with heat and light. In this application, a tank filled with water channels the SW towards cell specimens submerged at the opposite end. This study describes the design of a benchtop SW generator (SWG) for *in vitro* models and the optimization of bridge wire properties to render the platform tunable.

2 BACKGROUND AND LITERATURE

2.1 SHOCK WAVES AND BIOMECHANICS

A blast wave is an SW generated by explosives. In the physics domain, an open-field SW is characterized by the Friedlander waveform, which is visualized in Figure 2. Prior to the SW, the air pressure is in equilibrium at ambient pressure, p_0. When the shock front arrives at t_A, the pressure instantaneously jumps from ambient to the peak overpressure, p_{max}. In reality, this jump is not instantaneous and the time it takes to go from p_0 to p_{max} is defined as the rise time.

The pressure then follows a quasi-exponential decay back towards p_0. This decline often oscillates, crossing the p_0 a few times before coming back to equilibrium. Each region generated by crossing the equilibrium point is considered a phase.

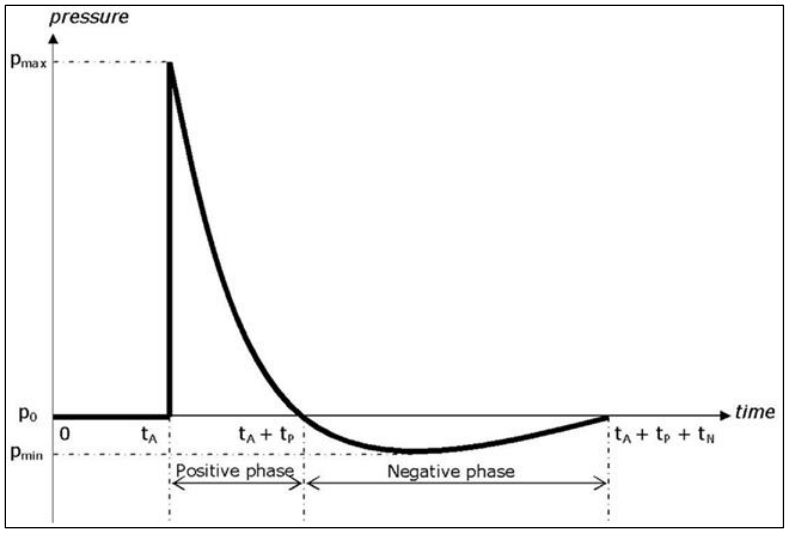

Figure 2. Friedlander waveform describes the pressure of the fluid medium in an ideal open-field blast event. Three time points are noted in the figure: t_A is the time of arrival, t_P is the time of the positive phase, t_N is the time of negative phase. p_{min} and p_{max} are pressure values that occur in the positive and negative phase, respectively. p_0 is the ambient pressure [27]

From this waveform, a handful of biomedically relevant metrics can be derived [28]. The first positive phase and first negative phase contain the p_{max} and p_{min}, respectively and their durations were one of the first metrics used to identify injury [29]. By integrating the pressure curve over these durations, the impulses of the positive and negative phases are identified. These new metrics provided insight into the compression and expansion stresses felt by tissue, evolving the durations into a more informative feedback metric [30], [31]. The rise time has also been shown to be a valuable metric for injury, as it encompasses the largest change in stress the body experiences during the shock event.

The peak overpressure, p_{max}, is the simplest metric to determine and has been used as the primary reporting metric in journals, along with positive duration, for conveying severity, particularly in the blast-induced TBI (bTBI) field [32]. Positive impulse has also become a popular metric, which combines the peak overpressure and positive duration. However, the relationships between each of these metrics and the variety of injuries sustained are not well understood and is the motivation for primary blast injury research. This research is further complicated by the lack of quantifiable data available from blast exposures.

In bTBI research, the severity of these injuries is traditionally classified by the symptoms presented by those exposed. Recent efforts have aimed to quantify the injury with the pressure metrics gleaned from the blast waves and other exposure statistics related to the individual. While this type of quantification of injury is not yet standard, there have been efforts to correlate the variety of available SW metrics with specific injuries. In 2009, Champion et al. compiled the peak overpressures required to cause eardrum rupture, lung injury, and death in humans [11]. They found that by 15psi, eardrums were likely to rupture, by 80psi, lung damage was likely to occur, and a 50% chance of death becomes possible at 130psi. Other efforts aim to identify the peak overpressure metrics associated with occupational blast exposure, which tend to expose servicemembers to repeated, low peak overpressures. In these instances, peak overpressures from a single exposure are as low as 5psi up to 20psi [4], [33].

2.2 ELECTRICAL EXPLOSION OF WIRES

When a pulse of high energy is supplied to a bridge wire, the high concentration of energy excites the atoms that make up the wire and causes the wire to expand. In the EEW process, the energy is high enough to cause the wire to change states of matter, from its original state as a solid, into a liquid, and eventually a gas or plasma. Because discharge is largely unresisted by the circuit, this change of state occurs in microseconds. The onset of the gas or plasma channel causes the electrical current to drop, as the new state of matter is resistant to electron flow. Further energy deposited into the gas or plasma channel transfers the electrical energy as optical emissions and SWs. In 2017, Han et al. found that the energy deposited before the peak voltage directly correlated with the amount of energy converted to the SW [34]. Experimentally, approximately 10% of the energy transfers into the SW that propagates through the surrounding media [35].

Currently, EEW is used for various commercial and research applications. Due to the bridge wire's small size relative to its explosive potential, the process has been of prioritized interest for oil reservoir stimulation [36]. Nano powder generation and non-thermal food processing have also found the process

to be applicable [37], [38]. The process's application has become an informative tool for relatively efficient plasma science research [39].

2.3 PULSED POWER GENERATORS FOR EEW

While pulsed power generators (PPG) take many forms and variations, they can be generalized to the circuit shown in Figure 3, which features two subcircuits. In the charging subcircuit, a power supply generates a voltage differential in the capacitor. A relay or set of relays is installed that ensures that only one subcircuit is engaged at a time and is visualized in Figure 3 as a single pole, double throw (SPDT) relay with a normal state closing the charging subcircuit. When triggered, the relay simultaneously disengages the charging subcircuit and engages the discharging subcircuit and the energy in the capacitor is released through the load. This generates the short burst of energy characteristic of PPGs and required by EEW.

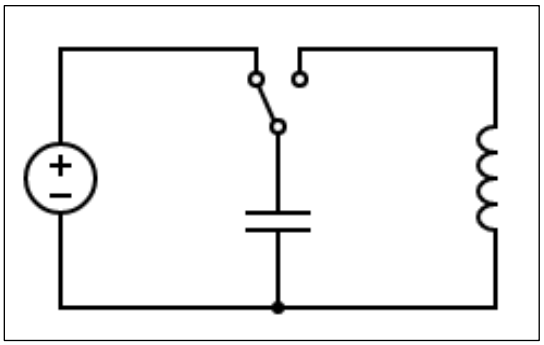

Figure 3. Generalized schematic for PPGs. The voltage source charges the capacitor. Once triggered, the SPDT flips and discharges via the load, represented here as an inductor. Often, this basic model is adapted and modified for the particular application.

For the application of EEW, the generalized pulse circuit schematic requires little modification [40], [41]. Most changes are additions for the purpose of safety, monitoring, and control. However, the specifications for each component must be carefully selected for optimal and consistent performance. To generate a strong SW consistently, the circuit must deposit enough energy in a short amount of time to completely vaporize the bridge wire, E_{vap} [42]. Notably, rapid deposition is related to low capacitance [43], [44]. The energy stored in a capacitor, E_{cap}, is defined by the capacitance, C, and the voltage, V.

$$E_{cap} = \frac{1}{2} C V^2$$

Given the demand for high energy and rapid deposition, the capacitor used in an EEW PPG must have a low capacitance and high allowable voltage. The high voltage power supply (HVPS) must be able to supply voltages that charge the capacitor such that $E_{cap} >> E_{vap}$ [43]. The description provided is all in relative terms because the vaporization energy, E_{vap}, is wholly dependent on the bridge wire.

2.4 INFLUENCE OF BRIDGE WIRE PROPERTIES ON EEW

The circuit design and the wire properties work together to generate an SW. As described above, the circuit provides the energy to break the wire, but the amount of energy required is defined by the wire's material and volume.

Each material has a set of thermophysical properties that determine the amount of energy required to vaporize the wire [45]. The specific enthalpy of vaporization is defined as

$$S_{vap} = S_{h,s} + S_{LHF} + S_{h,l} + S_{LHV}$$

Where $S_{h,s}$ is the enthalpy required to heat the solid from 298K to the melting point, S_{LHF} is the latent heat of vaporization, $S_{h,l}$ is the specific enthalpy required to heat the liquid form the melting point to the vaporization point, and S_{LHV} is the latent heat of vaporization per mass. The specific enthalpy of heating, S_h can also be defined further relative to the Shomate equation for a material's specific heat, c_p. The vaporization energy for a given bridge wire (E_{vap}) can then be calculated using the specific enthalpy of vaporization, the mass density (ρ), and the initial volume of the bridge wire (V_0).

$$E_{vap} = S_{vap} * \rho * V_0$$

While vaporization is necessary to generate an SW with a basic level of consistency, further criteria provide opportunities to strengthen the SW and ensure reproducibility. Han et al. examines various discharge types based on their electrical current profiles and finds that two current spikes exist, which can be separated by a dwell caused by high resistivity brought on by the dense plasma or gaseous state [34].

These separated current spikes limit the peak power that can be produced, resulting in weaker SWs. By increasing the wire volume, they found that the current dwell could be eliminated resulting in stronger SWs [46].

Further, evidence suggests that energy deposition early in the vaporization process, as opposed to the channel expansion and breakdown stages that occur afterward, correlates with higher amplitude SWs [34], [43], [47]. This early deposition can be obtained by increasing the initial wire volume and selecting materials with low resistivity as plasmas and gases, where possible [48]. A positive relationship between vaporized mass and SW overpressure was also identified, suggesting increases to the bridge wire volume for more power SWs [42]. Collectively, these findings suggest that wires with larger volumes have the potential to generate stronger SWs than their thinner counterparts.

2.5 WATER-MEDIATED SHOCK WAVES

There are a couple benefits to using water as the medium for wave propagation. When in the air, the SWs produced by the EEW are sensitive to imperfections on the surface of the wire [45]. In water, the flashover effects that result from these imperfections are greatly suppressed due to the compression of the water and [49]. Moreover, the uniformity of the plasma or gas channel is greatly improved by the compression of the water. For these and other reasons not pertinent to this research, underwater electrical wire explosion (UEWE) has become a popular variant of the EEW process [46].

From a biomechanics perspective, the water acts as a more comparable intracranial wave propagator than air for *in vitro* TBI models. When an individual is exposed to a blast wave, the blast wave is transformed upon entry into the brain, changing pressure metrics like the peak overpressure and rise time [50], [51]. While an air-mediated environment would be capable of simulating the transformed wave, the large difference in acoustic properties between air and the tissue would not accurately represent the injury environment of the cells. Water much more closely resembles the acoustic properties of brain tissue, enabling the SWG to deliver SWs in an environment that resembles the intracranial environment.

2.6 PLATFORMS FOR BLAST INJURY RESEARCH

Initial blast research efforts developed the open-field blast platform, where models or surrogates were placed in an open area near explosives [52]. In the past few decades, blast tubes have presented a less variable and more controlled method of testing free-field blasting. However, blast tubes do not inherently generate SWs comparable to those experienced in the field and improper design and operation of the blast tubes can lead to erroneous conclusions [53]. ABSs have been designed with these considerations in mind and have produced systems applicable for surrogate and animal models.

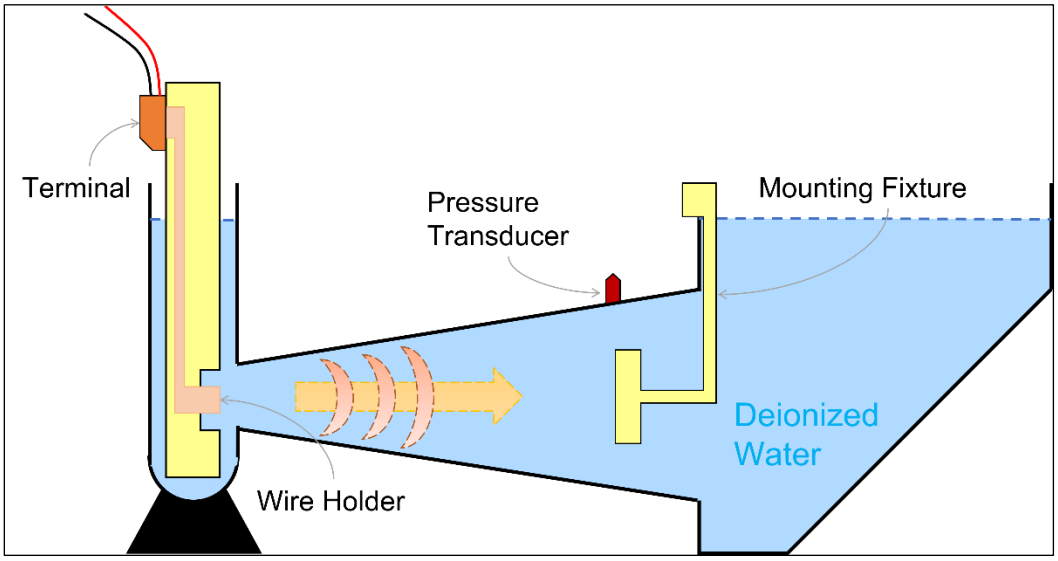

Figure 4. Diagram of the SWG tank, with blast board and well plate holder inserted. As the wire, mounted at the bottom of the blast board in the wire holder, vaporizes, an SW is generated and propagates down the tube towards the specimen mounted in the well plate. Pressure transducers on the wall and well plate mounting fixture measure the SW.

In 2013, Hampton et al. introduced the first known system designed for *in vitro* blast injury, specifically bTBI [26]. A diagram of the SWG is shown in Figure 4. Using a UEWE design, the SWG generated an SW at one end of the tank. The wave propagated down the tank towards a well plate positioned in the center of the tank, causing injury to the specimen. The pressure transducer in the wall recorded the SW's static pressure. The system has been used for subsequent studies and has provided the primary blast injury community with a platform for *in vitro* investigations [16], [18].

In 2020, the PPG was redesigned and outfitted with updated and new components, including the HVPS, triggering relay, bleed resistor, voltage probe, and capacitor. The current state as of this thesis is detailed in Figure 5. The footprint of the whole system is a two and a half foot by nine-foot benchtop area, with the SWG tank taking up four of the nine feet. The cells are placed in a variety of mounting fixtures, including 6-well plates (Corning, Costar 3516) or suspended in hydrogels and placed in three inches by three-inch heat-sealed bag filled with cell culture media (ScienCell, Astrocyte Medium #1801). A single hydrogel or well plate typically contains 150,000-500,000 cells upon seeding.

There are limitations to the current state of the SWG, particularly as it relates to the medium. In Figure 7, a negative phase is present prior to the wave's arrival. This deviation from Friedlander waveform is suspected to be caused by the relative incompressibility of water compared to air and the fully enclosed tank. Further investigation of both the mechanism causing this generation as well as the injury implications of this negative phase are necessary.

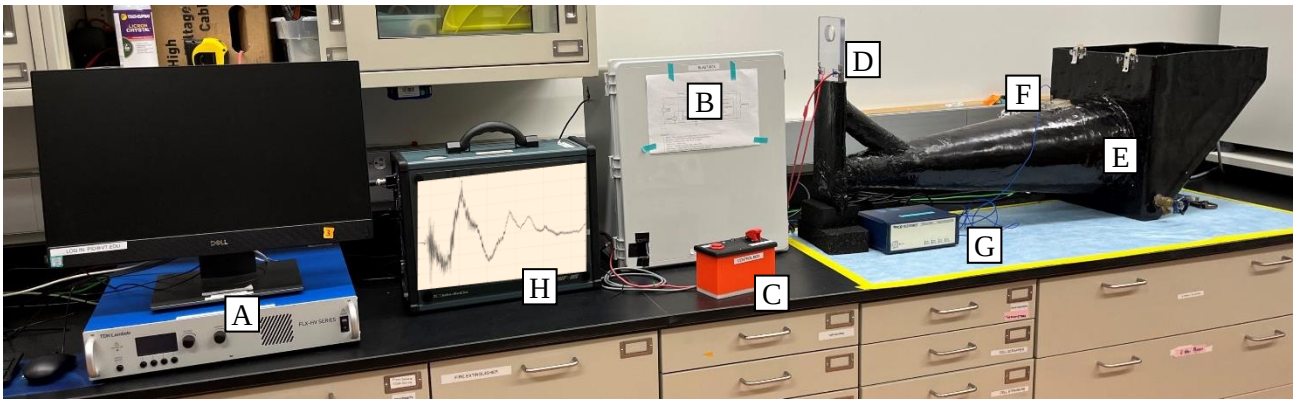

Figure 5. Current State of Shock Wave Generator. The HVPS (A) charges the pulse capacitor, housed in the Blast Box (B). The operator triggers detonation using the control panel (C), discharging the capacitor through the blast board (D), where the bridge wire is mounted. The bridge wire explodes, and the SW travels down the SWG tank (E) towards cells fixed in the tank. The pressure transducer (F) reads the pressure change, relays the signal to the signal conditioner (G), before being recorded by the data acquisition system (H).

3 METHODS AND MATERIALS

3.1 PPG CIRCUIT DESIGN

The PPG circuit was based on the system described in Hampton et al., with adaptations that increase precision, reinforce safety, and provide more feedback to the operators [26]. The HVPS (TDK Lambda FLX10P20) charged a 2uF, 5kV max capacitor (General Atomics 37600, Figure 6A). A SPDT relay (Ross Engineering Corp E15-DT-15-1-0-BH, Figure 6D) was placed such that the naturally closed throw connected to the HVPS, and the naturally open throw connected to the bridge wire. A high voltage (HV) probe (Fluke 80K-6, Figure 6B) actively measured the voltage stored in the capacitor and recorded and displayed the readings on the data acquisition system (DAQ, AstroNova DASH-8HF). A bleed resistor (Ohmite MOX-G-022504FE, Figure 6C) was installed across the capacitor terminals to ensure the complete discharge of the capacitor.

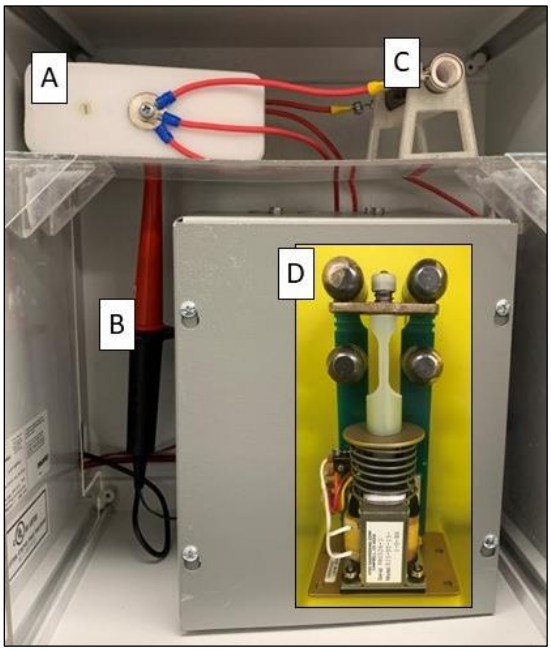

Figure 6. Circuit Components of the PPG, contained within the Blast Box. The HVPS (not seen here) charged the 2uF capacitor (A). The HV probe (B) relayed the current voltage to the operator. Once the capacitor was charged, a trigger signal was sent to the HV SPDT relay (D), discharging the capacitor. The bleed resistor (C) shorted the two terminals of the capacitor, ensuring the capacitor was discharged unless it was actively charging.

Once the capacitor was charged to the desired voltage, the operator sent a signal to the HV relay that disengaged the subcircuit containing the HVPS and engaged the subcircuit with the bridge wire. In tens of microseconds, the capacitor was discharged across the bridge wire. After the bridge wire broke, any remaining voltage in the capacitor was discharged via the bleed resistor.

3.2 SHOCK WAVE CAPTURE

The DAQ captured two signals over the course of the shock event at 1MHz for 1 second. First, the capacitor voltage was recorded from the voltage probe. The pressure was recorded using a piezoelectric pressure transducer (PCB Piezotronics, 113B21) and was mounted in the wall of the SWG tube to capture the static pressure at the specimen. The pressure transducer was connected to a signal conditioner (PCB Piezotronics, 482C15) before being relayed to the DAQ.

The DAQ was triggered off a signal relayed by the control box. A redundant rising-edge trigger was set based on the pressure transducer to ensure capture. Once the blast testing was complete, the proprietary data files were exported via an external hard drive. Using AstroViewX, the proprietary data file was converted to a CSV containing the data and metadata.

3.3 BLAST PROCEDURE

The SWG tank was filled with deionized water and heated to approximately 37°C by rotating the water through kettles. The HVPS and the desktop used to control the HVPS were booted up, and the controlling software was opened, connected to the HVPS, and the charging script was uploaded. The DAQ and signal conditioner were booted up. The pressure transducer was connected to the signal conditioner and tested to confirm it was responding properly. The key switch was turned on.

The terminals on the blast board were disconnected and the board was removed from the SWG tank. A wire approximately 13cm long was cut, was pulled hand taught, and clamped into the blast board. No further processing was conducted on the wire. After excess wire was trimmed, the blast board was

reinserted into the SWG, and the terminals were reconnected. Once all participants were ready, the toggle switch was engaged and the DAQ was armed.

The charging script for the HVPS was run, supplying 5kV at 20mA and displaying the voltage of the capacitor on the DAQ. When the capacitor voltage plateaued at 4.7kV, the button switch was pressed. With the key switch engaged, toggle switch engaged, and the button pressed, a trigger signal is simultaneously sent to the DAQ and the HV relay, opening the charging circuit and closing the discharge circuit.

Upon vaporization the DAQ was triggered. The toggle switch was disengaged, ensuring the discharge subcircuit is open and safe for handling. When another test was to be run, the wire would be replaced, and the system's protocol was repeated.

Once all testing was complete, the key switch was disengaged. The SWG tank was emptied. The desktop was programmatically disconnected from the HVPS, the software was closed, and both the desktop and HVPS were turned off. The signal conditioner was turned off and the sensors were disconnected. All data collected on the DAQ was exported using a portable hard drive and the DAQ was subsequently shut down.

3.4 SHOCK WAVE METRICS EXTRACTION

A MATLAB script (MathWorks MATLAB R2021b) was developed to analyze the captured pressure curves and extract the various pressure metrics that inform injury. After importing the pressure data, the script located five key time-points along the shock curve: Arrival (t_a), First Zero Intersect (t_{01}), Peak Overpressure (t_{max}), Second Zero Intersect (t_{02}), and Third Zero Intersect (t_{03}). These points are visualized in Figure 7. In an air-mediated Friedlander waveform, t_a and t_{01} would coincide but the current SWG design generated the negative phase prior to the peak overpressure. Each of the intersects represented the ending of one phase and the beginning of the next, alternating between positive and negative phases. In theory, this identification of alternating phases could continue until there was a return

to ambient pressure. However, injury was hypothesized to occur within the first positive and negative phases, drawing the limit used here.

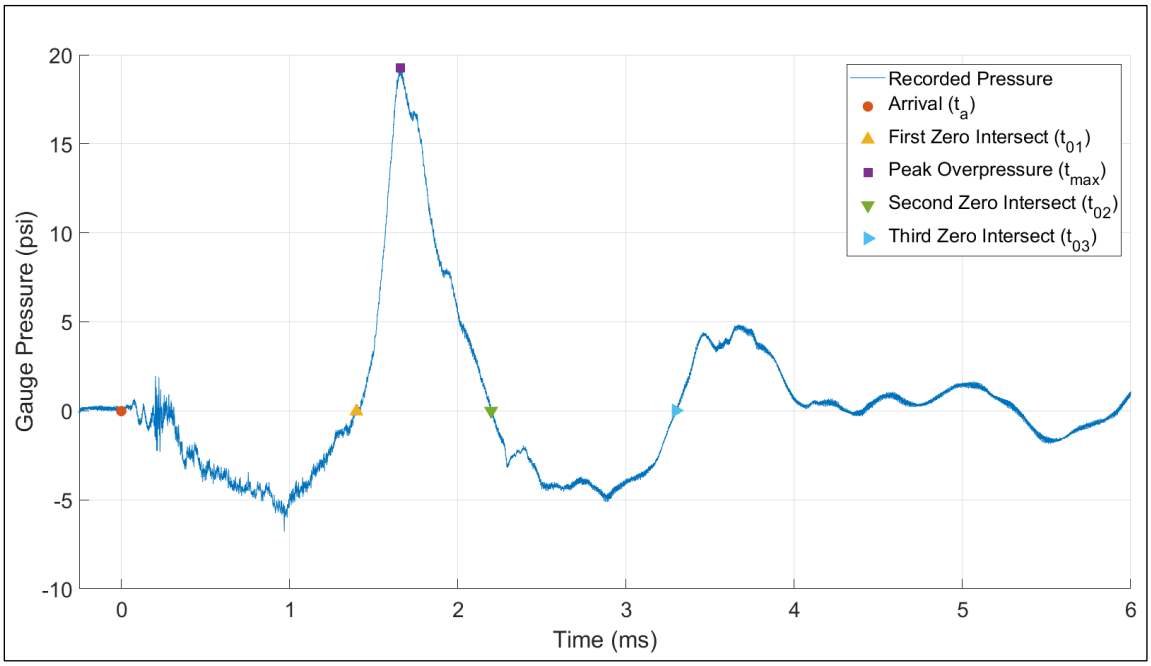

Figure 7. A typical pressure curve recorded from a UEWE event. The five key time-points are marked according to the legend in the top right of the figure.

These five values were then used in various combinations to calculate the pressure metrics for the shock curve, as defined in Table 1. The arrival time, t_a, served as the reference point for the Friedlander curve in the captured data at large and the end point for the range used to zero the data.

Table 1. The relationships between the key time-points and pressure metrics, along with the reporting units for each metric. P() was the recorded pressure

Pressure Metric	**Calculation Based on**	**Reporting Units**
Peak Overpressure	$P(t_{max})$	Pound Square Inch (psi)
Rise Time	$t_{max} - t_{01}$	Milliseconds (ms)
Positive Duration	$t_{02} - t_{01}$	ms
Positive Impulse	$\int_{t_{01}}^{t_{02}} P(t)dt$	psi*ms
Negative Duration	$t_{03} - t_{02}$	ms

Negative Impulse	$\int_{t_{02}}^{t_{03}} P(t)dt$	psi*ms

The MATLAB script iterated this process over all submitted shock curves. The metrics were exported via an Excel Workbook. The MATLAB script also saved a figure of the shock curve, like the one in Figure 7.

3.5 WIRE EXPERIMENTATION

Five materials (Copper, Nichrome, Silver, Tungsten, and Stainless Steel) and three diameters of wire (32 AWG, 36 AWG, 40 AWG) were selected to be tested. The diameter represents the volumetric parameter because the remaining dimension, length of wire, was constant for all wires. Previous studies with this system and pilot studies suggested that wires with diameters larger than 32AWG failed to completely vaporize consistently, regardless of material [26]. Given the literature review and pilot studies, the five materials were selected due to their breadth of material properties [48], commercial availability, and potential to generate SWs in peak overpressure ranges of biomechanical interest [26]. A power analysis was conducted and recommended that a sample size of five for each combination of wire diameter and material, resulting in seventy-five total trials.

Table 2. The combination of wire diameter and wire material. Each combination has an associated shorthand, defined in the table.

	Copper (Cu)	**Nichrome (NiCr)**	**Tungsten (W)**	**Stainless Steel (SS)**	**Silver (Ag)**
AWG 32	Cu32	NiCr32	W32	SS32	Ag32
AWG 36	Cu36	NiCr36	W36	SS36	Ag36
AWG 40	Cu40	NiCr40	W40	SS40	Ag40

3.6 Statistical Analysis

Two-way ANOVAs were performed using JMP (JMP Pro 16.0.0). The material and diameter were independent, categorical variables. While the material was intrinsically categorical, the diameter was treated as ordinal but categorical due to the use of standardized diameters of the wire. The peak overpressure, positive duration, and positive impulse were analyzed independently as dependent variables. These were chosen because the peak overpressure and positive duration are the primary metric reported for injury analysis while positive impulse is gaining popularity as the reporting metric. A Tukey-Kramer HSD Paired Means Comparison (TKPMC), an alternative to a paired t-test that considers family-wise error rates, was conducted to compare the shock metrics achieved by different diameters and materials. Three sets of three TKPMCs were performed, one for each of the main effects and a third for the interaction effect for each shock wave metric.

4 Results

4.1 Peak Overpressure

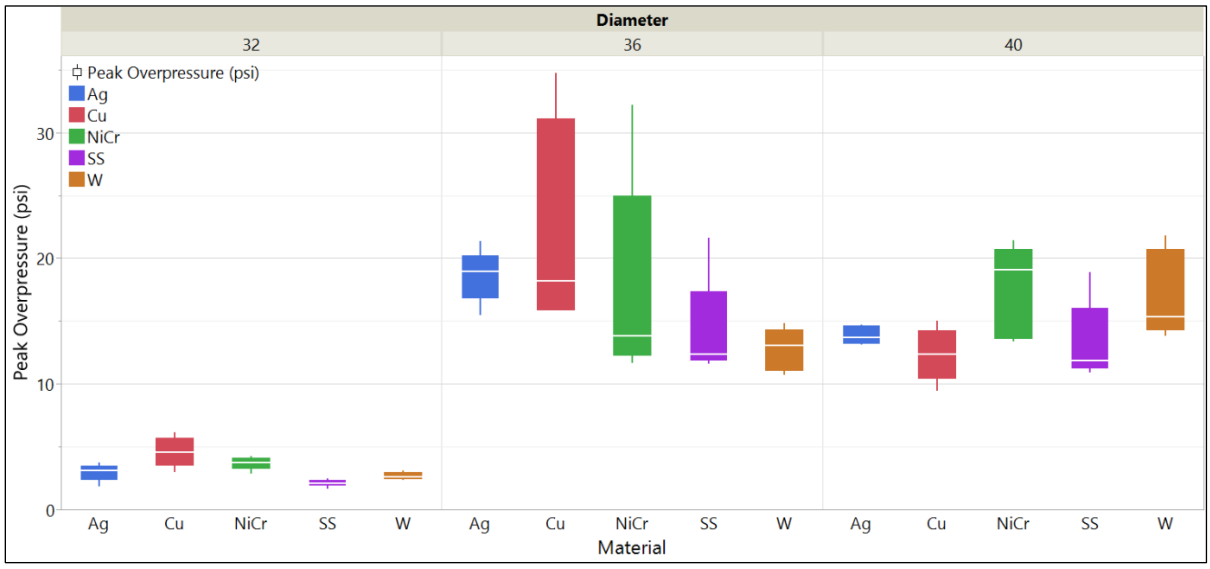

Figure 8. Peak overpressure relative to the diameter and material of the wire. Each group has n=5.

The two-way ANOVA for peak overpressure was conducted to compare the main effects of wire material and diameter and their interaction effect on the peak overpressure. Wire material was not found to have a statistically significant effect on peak overpressure ($F(4,116.8751) = 2.0807$, $p = 0.0945$).

The analysis concluded that wire diameter had a statistically significant effect on the peak overpressure ($F(2,2780.2845) = 98.9932$, $p<0.0001$). The interaction of wire material and diameter was found to have a statistically significant effect on peak overpressure either ($F(8,302.9666) = 2.6968$, $p = 0.0133$). The least squares mean plots are shown in Figure 9.

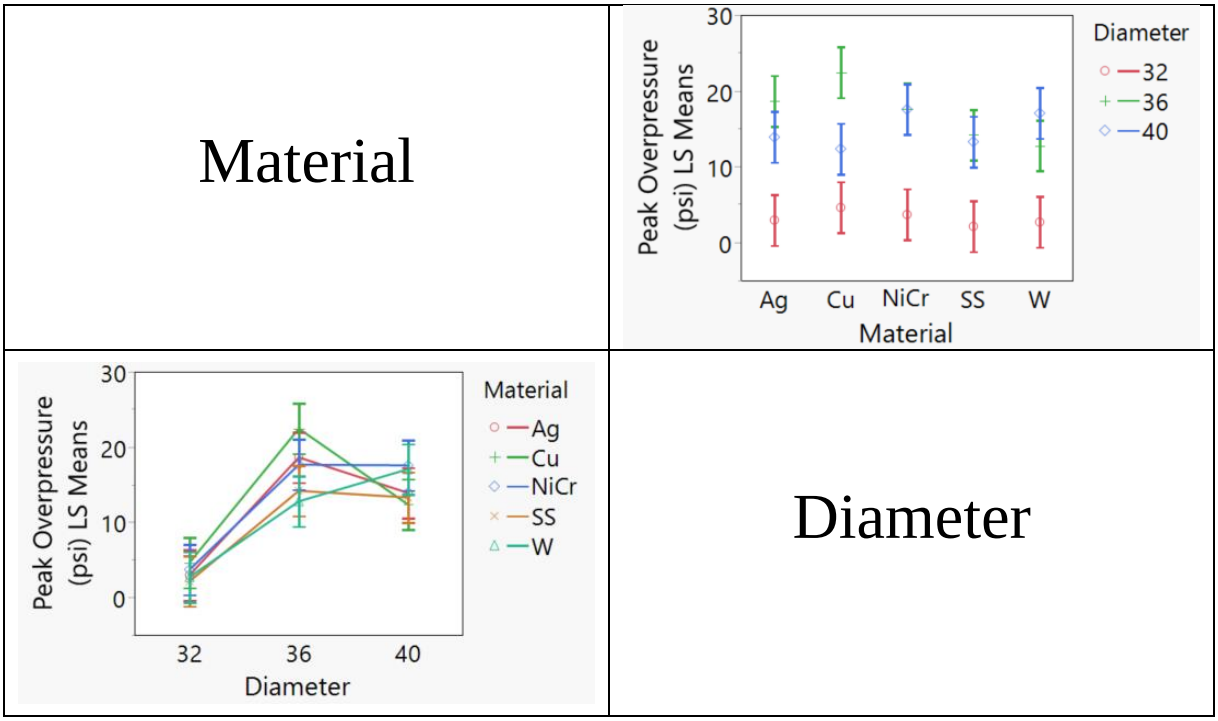

Figure 9. The least square means plots for the interaction effects of diameter and material.

The TKPMC for wire diameter reinforced the suggested impact of diameter on peak overpressure, noting a statistical significance between 32 AWG and both 36 AWG ($p<0.0001$, 95% C.I. = [11.3666,16.461]) and 40 AWG ($p<0.0001$, 95% C.I. = [9.05959,14.154]). There was no statistical significance between 36 AWG and 40 AWG wire ($p = 0.1328$, 95% C.I. = [-4.8542,0.24023]). The TKPMC for wire material did not identify any statistically significant difference between materials.

The TKPMC for the interaction effect, which compared every combination of wire material and diameter resulted in 105 pairs. Of these pairs, fifty-two were found to be significantly different from one another. Notably, forty-eight of these fifty-two were between a 32AWG wire and a 36AWG or 40AWG wire, corresponding to the findings of the diameter TKPMC. All TKPMC pairs and their related statistics, including p-values for both main effects and the interaction effect are in Appendix A.1 for peak overpressure.

4.2 POSITIVE DURATION

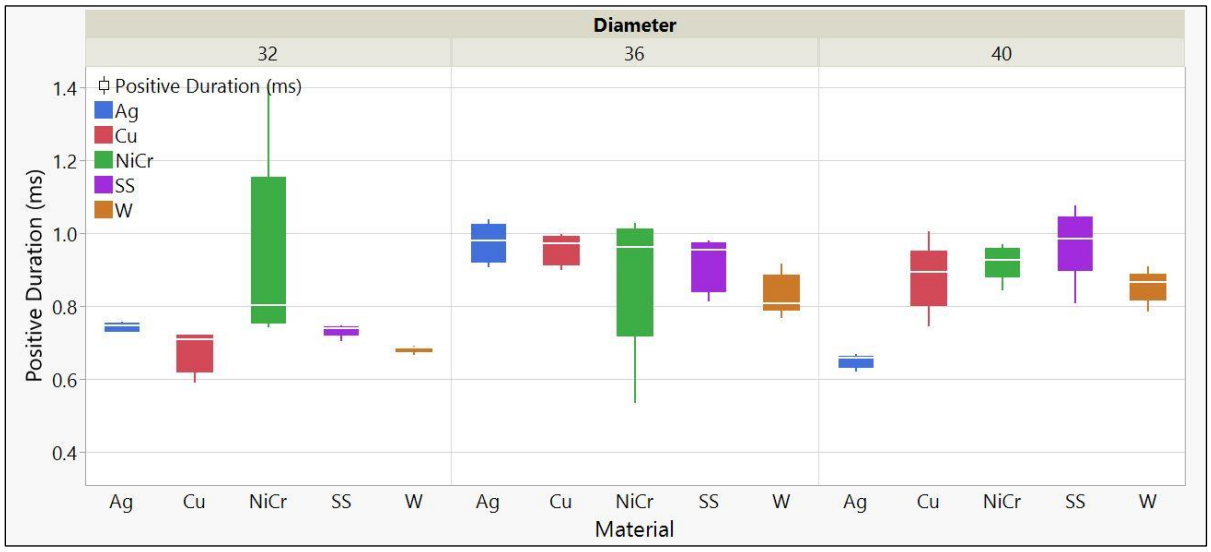

Figure 10. Positive Duration relative to the diameter and material of the wire. Each group has n=5.

As second two-way ANOVA was conducted to compare the main effects of wire material and diameter and their interaction effect on the positive duration. Both of the main effects and the interaction effects were found to be statistically significant on positive duration (Material: $F(4,0.1679) = 3.9520$, $p = 0.0065$; Diameter: $F(2,0.3314) = 15.6063$, $p < 0.0001$; Material*Diameter: $F(8,0.4065) = 4.7851$, $p = 0.0001$).

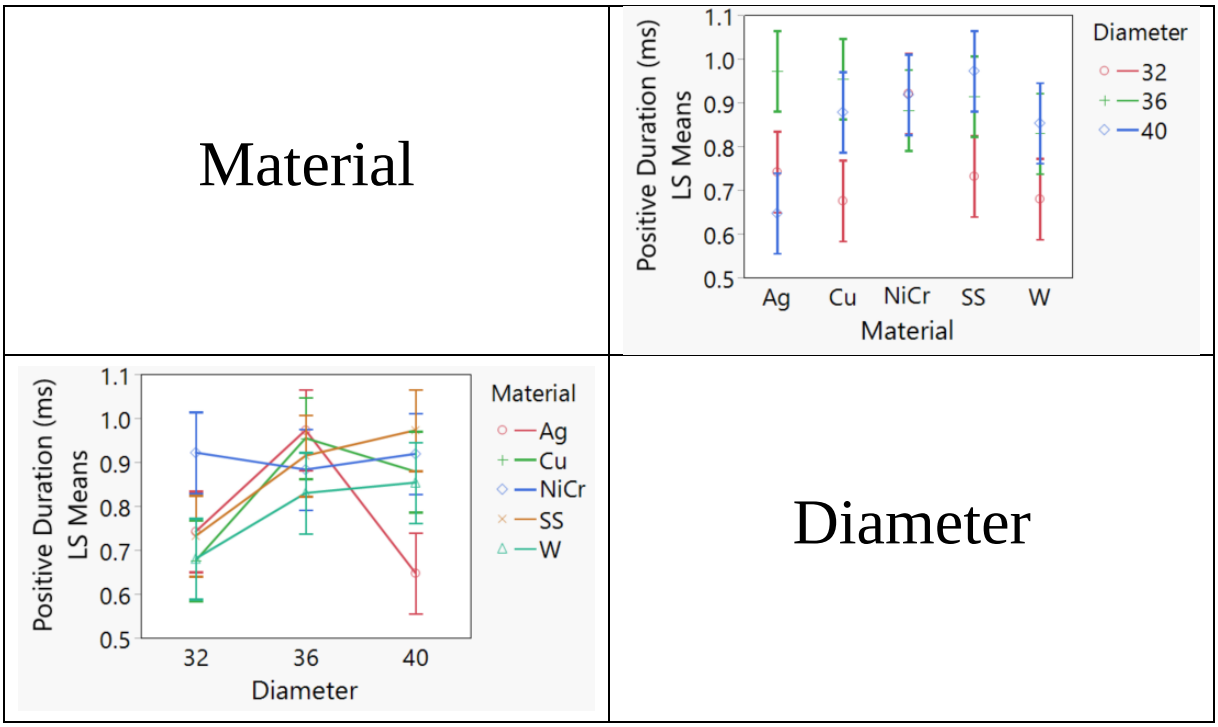

Figure 11. The least square means plots for the interaction effects of diameter and material.

The material's significance seems to be mostly derived from the statistically significant difference between nichrome with silver (p = 0.0180, 95% C.I. = [0.014575,0.2262251]) and nichrome with tungsten (p = 0.0185, 95% C.I. = [0.014242,0.2258918]). All other combinations were not found to be statistically significant.

Like peak overpressure, the diameter of the wire had a significant impact between 32 AWG and both 36 AWG (p<0.0001, 95% C.I. = [0.090516,0.2306042]) and 40 AWG (p = 0.0021, 95% C.I. = [0.033716,0.1738042]). There was no statistical significance between 36 AWG and 40 AWG wire (p = 0.1340, 95% C.I. = [-0.013244,0.1268442]).

All TKPMC pairs and their related statistics, including p-values for both main effects and the interaction effect are in Appendix A.2 for positive duration.

4.3 POSITIVE IMPULSE

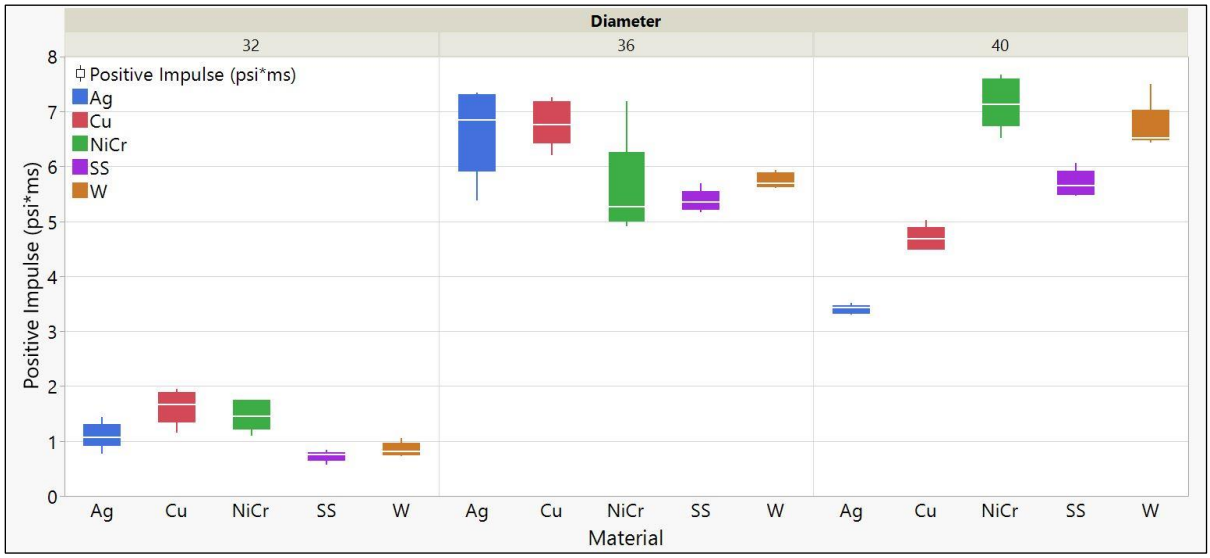

Figure 12. Positive Impulse relative to the diameter and material of the wire. Each group has n=5.

A third two-way ANOVA was conducted for positive impulse to compare the main effects of wire material and diameter and their interaction effect. All effects, main and interaction, were found to be statistically significant for positive impulse (Material: $F(4,9.88925) = 14.6246$, $p < 0.0001$; Diameter: $F(2,359.52825) = 1063.372$, $p < 0.0001$; Material*Diameter: $F(8,48.30346) = 35.7166$, $p < 0.0001$).

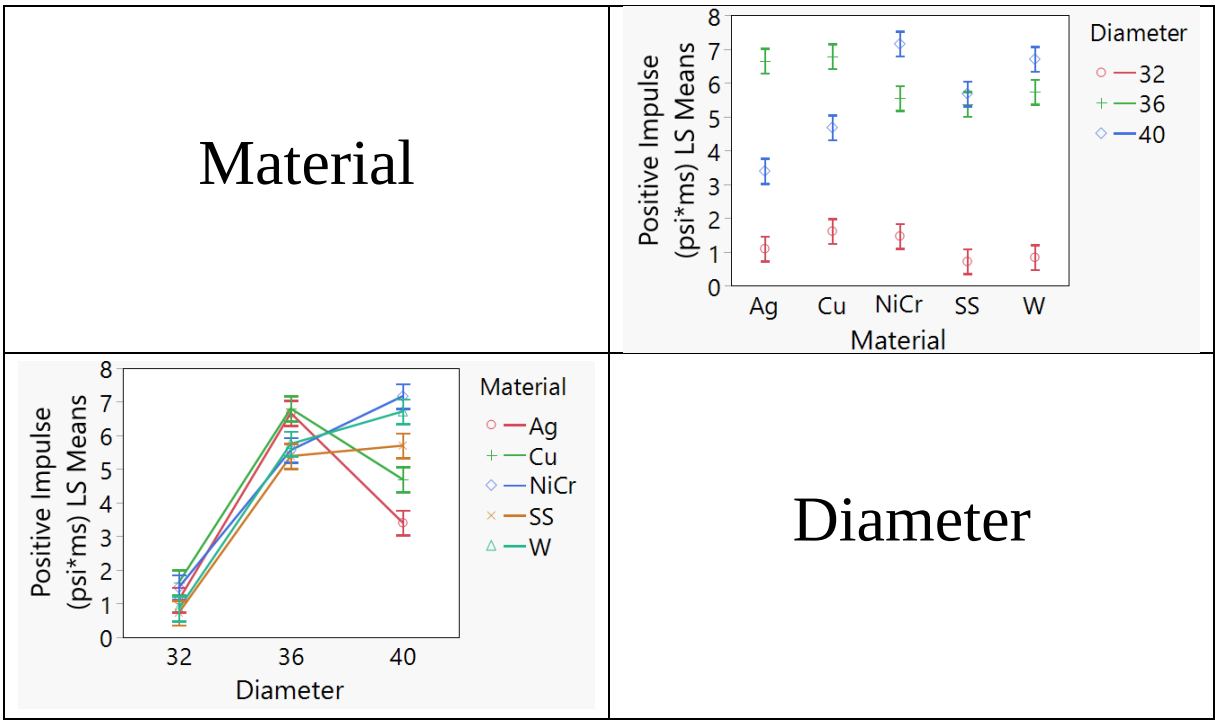

Figure 13. The least square means plots for the interaction effects of diameter and material.

For material as the main effect, two groups formed with significant separation. Stainless Steel and Silver were significantly different than Nichrome, Tungsten, and Copper but there were no significant differences within these two described groups.

Breaking with the trend set by peak overpressure and positive duration, all three diameters were significantly different than one another, as seen in Appendix A.3.2. The interaction effects continued to reflect that 32 AWG wires were different from 36 AWG and 40 AWG wires. Within the combinations of diameter and material, no notable correlations were found, though significance between combinations was common. All TKPMC pairs and their related statistics, including p-values for both main effects and the interaction effect are in Appendix A.3 for positive impulse.

5 DISCUSSION

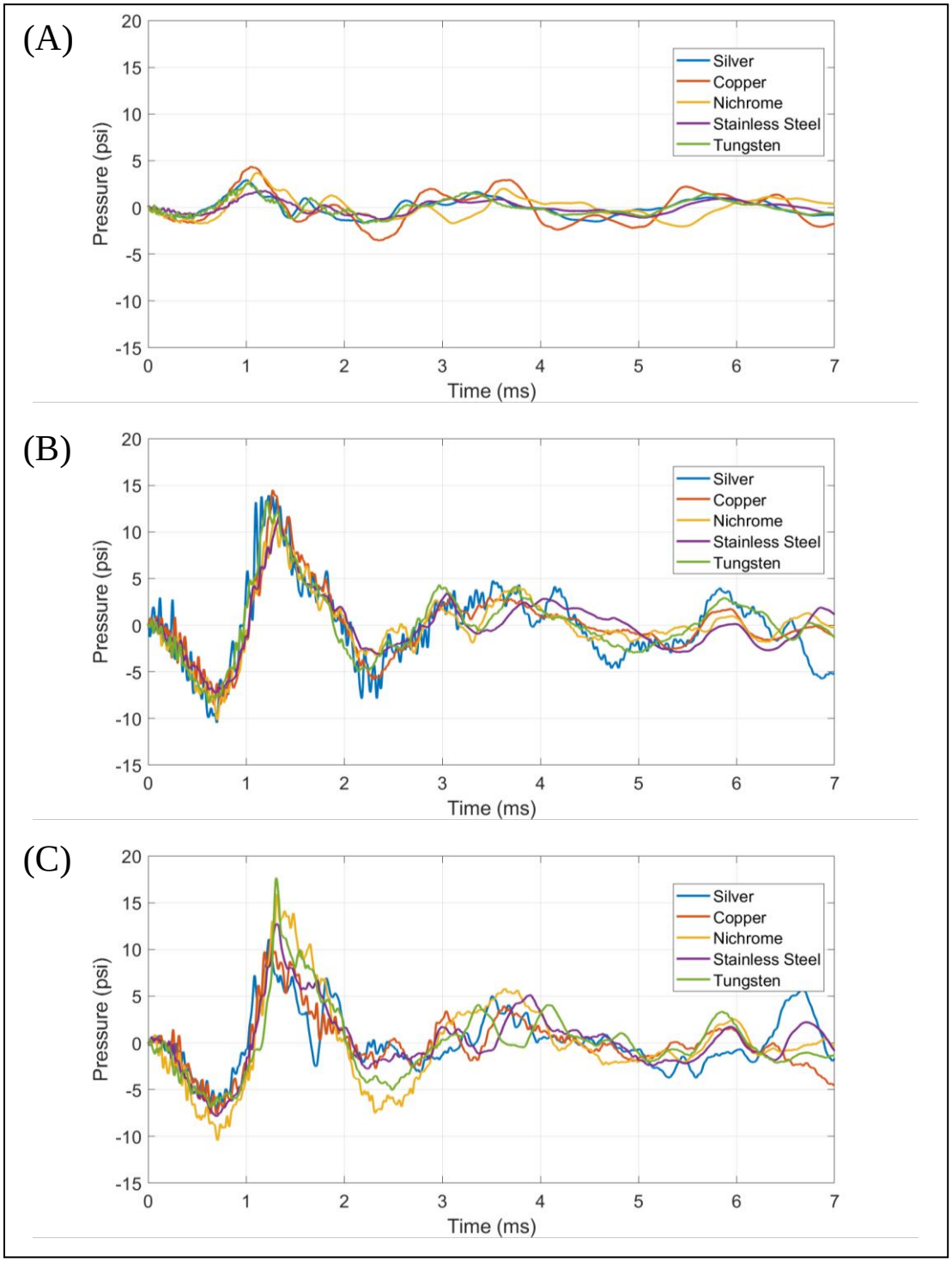

Figure 14: Captured pressure curves for each material for (A) 32 AWG, (B) 36 AWG, and (C) 40 AWG diameter wire. All data was post-processed with a 10 kHz lowpass filter.

5.1 BLAST WAVEFORMS

In Figure 14, waveforms for all fifteen combinations of wire diameter and material were compared. No major discrepancies were noted between materials at a given diameter. It was observed that the materials demonstrated more variability at 40 AWG compared to the 32 and 36 AWG groups.

5.2 IMPACT OF DIAMETER

Overall, the diameter seemed to be the leading indicator for the pressure metrics considered here. From 32 AWG to 36 AWG, a noticeable increase occurred. 36 AWG and 40 AWG then showed a plateau or slight decline in the given metric. Both of these steps correlate to a pair of understood phenomena related to EEW apparatuses, especially those that utilize low energy PPGs.

Regardless of material, there was a statistically significant increase in the peak overpressure between 32 AWG and 36 AWG. This correlates with the concept of overcoming the vaporization energy of the wire [42]. In Berning and Coppinger, they calculated that the energy required to vaporize a copper wire from 25°C is approximately 55.25 kJ/cm^3 [45]. Given the wire is set at 3cm long, the vaporization energies for 32, 36, and 40 AWG diameter copper wires are 20.3J, 13J, and 7.3J, respectively. The current circuit components theoretically cap the potential energy in the capacitor at 25J but are likely supplying closer to 22J of energy. This means that the energy deposited into the wire has no margin, which Li et al. identifies as necessary for consistent and strong SWs. This concept is incorporated into a hypothesized curve drawn in Figure 15 as the vertical ‘Deposited Energy Limit’ line.

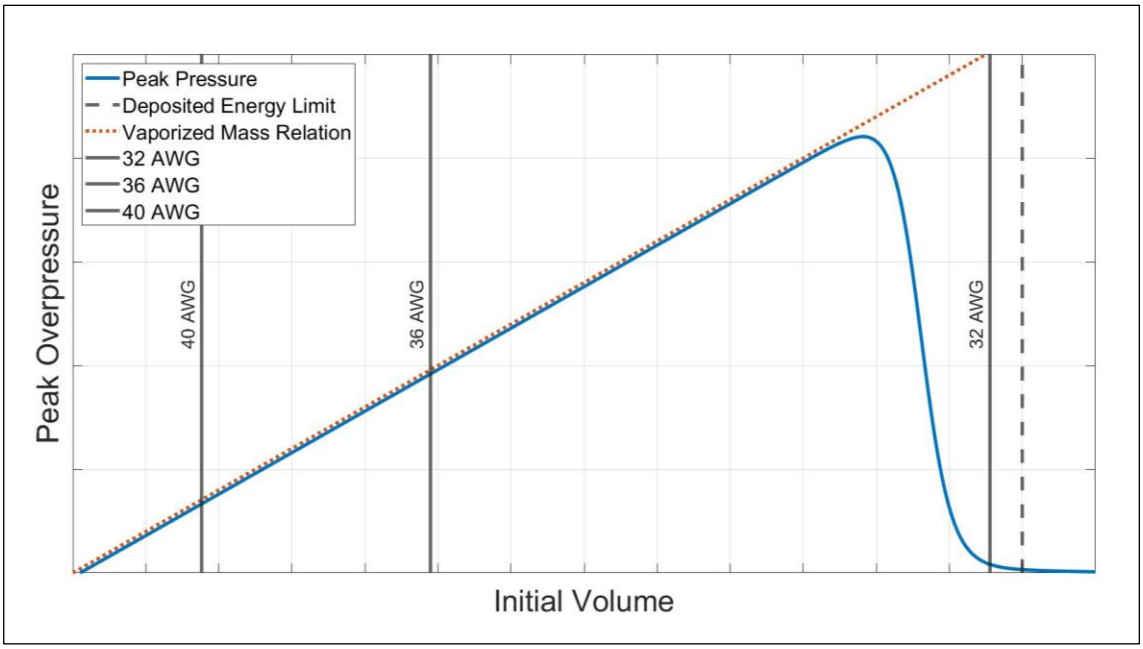

Figure 15. Proposed relationship between the initial volume of the material and the peak overpressure. The three diameters are separated to-scale.

The plateauing or even decrease in peak overpressure and positive duration between 36 AWG and 40 AWG wire may highlight the second phenomena. While reducing the wire diameter increases the energy margin described above, it also reduces the volume of material that is vaporized, a critical component to determining the translation of electrical energy into mechanical energy [42]. This limiting factor can be visualized with the 'Vaporized Mass Relation' line in Figure 15. Combining the two concepts described generates a hypothesized peak overpressure curve, labelled 'Peak Pressure' in Figure 15.

For application as an *in vitro* injury mechanism, the wire diameter is a promising feature for tuning the SWG. Diameter will be the leading determinant of the maximum amount of mass that can be vaporized. As it stands, overpressures in the mid- to high-teens (14-18 psi) and positive impulses in 6-8 psi*ms ranges can be consistently achieved with 36 and 40 AWG wires. Further optimization of circuit parameters will likely provide an opportunity for higher peak overpressures and positive impulses.

5.3 IMPACTS OF MATERIAL

Wire material does not have the same magnitude of influence over shock wave metrics that wire diameter does but does seem to have some impact on the resulting shock wave. Rarely did two materials perform identically for a given shock wave metric, much less identically across all three. This seems to suggest that the material may be modulating the shock wave. An example of this modulation can be imagined by scaling the 'Peak Pressure' plot in Figure 15 in both the x and y-axes.

It is also worth considering that the amount of material used is quite small, limiting the impacts of material properties. While it is well established that the specific heats for each phase and the latent heats for each state transition of a material play a role in the vaporization energy, these properties are always scaled by the amount of material present. By using volumes that are magnitudes smaller than the associated properties, the amount of material may be outweighing the effects of these properties. If vaporized mass were to increase, material properties would likely play a larger role and deserve more consideration.

While not investigated here, a variety of elements and alloys provide different combinations of thermoelectrical properties that may also provide higher degrees of consistency. Changes in resistivity as the material heats and changes states of matter can play pivotal roles in determining when electrical energy is deposited [45]. Qualitatively, this can be observed when comparing the performance of Tungsten or Silver to other materials like Copper and Nichrome relative to peak overpressure.

5.4 POTENTIAL IMPROVEMENTS

Increasing the voltage applied to the capacitor would permit a higher energy deposition. The capacitor's voltage rating limits the voltage applied to the capacitor, and thus the energy applied to the bridge wire. Replacement of the capacitor with one rated for higher voltages would provide a notable increase in the amount of energy supplied to the bridge wire and address the relative similarity between

the deposited and vaporization energies the current system configuration suffers from. A larger voltage range would also provide a third dimension for tuning, along with the wire material and diameter.

Changing the wire mounting mechanism could improve consistency. The current system relies on the tension of the installed wire to ensure contact between the wire and metal brackets. However, if the wire were not taut on the bracket, the wire may bow, increasing the length of the exploding section. This increased length increases the vaporization energy and likely changes the resulting SW.

Determining wave speed provides another injury-related mechanical metric along with validation of peak overpressure. The Rankine-Hugoniot relationship defines the relationship between an SW's speed and overpressure. Because ABS systems incorporate additional sensors, the speed of the wave can be calculated by dividing the difference between arrival times at each sensor by the distance of the sensors from one another. By installing additional static pressure transducers on the SWG tank, the Rankine-Hugoniot relationship can be utilized to verify the peak overpressures recorded by the pressure transducers.

Other capturing mechanisms may also be valuable in understanding the SW propagation and injury degree. While the current SWG tank could not accommodate an external camera, a new transparent tank would allow for video capture of the event. Pressure transducers facing the wave and mounted on or near the mounting fixture would also be able to capture the total pressure experienced by the cells.

While the controls of the system have greatly improved from their original state, additions can be installed to increase consistency, synchronize various processes, and provide more redundant safety features. An indicator light for the press of the detonation button could be added to standardize the voltage across the capacitor. Integration of the control panel with the HVPS controller could reinforce protections for the HVPS from the high current present upon discharge. Installation of a current probe would also be beneficial for the health of the system and future studies.

6 CONCLUSION

The UEWE proved to be a feasible method for generating SWs, providing the first-of-its-kind platform for *in vitro* primary blast injury. By altering the diameter of the wire, the SWG can generate various peak overpressures, allowing researchers to tune the system for various injury conditions. This platform has opened a new frontier for the investigation of primary blast injury.

REFERENCES

[1] B. D. Owens, J. F. J. Kragh, J. C. Wenke, J. Macaitis, C. E. Wade, and J. B. Holcomb, "Combat Wounds in Operation Iraqi Freedom and Operation Enduring Freedom," *J. Trauma Acute Care Surg.*, vol. 64, no. 2, p. 295, Feb. 2008, doi: 10.1097/TA.0b013e318163b875.

[2] N. Greer, N. Sayer, M. Kramer, E. Koeller, and T. Velasquez, *Prevalence and Epidemiology of Combat Blast Injuries from the Military Cohort 2001-2014*. in VA Evidence-based Synthesis Program Reports. Washington (DC): Department of Veterans Affairs (US), 2016. Accessed: Apr. 07, 2023. [Online]. Available: http://www.ncbi.nlm.nih.gov/books/NBK447477/

[3] A. J. MacGregor, A. L. Dougherty, and M. R. Galarneau, "Injury-Specific Correlates of Combat-Related Traumatic Brain Injury in Operation Iraqi Freedom," *J. Head Trauma Rehabil.*, vol. 26, no. 4, p. 312, Aug. 2011, doi: 10.1097/HTR.0b013e3181e94404.

[4] C. C. Engel, E. Hoch, and M. M. Simmons, "The Neurological Effects of Repeated Exposure to Military Occupational Blast: Implications for Prevention and Health: Proceedings, Findings, and Expert Recommendations from the Seventh Department of Defense State-of-the-Science Meeting," RAND Corporation, Mar. 2019. Accessed: Mar. 29, 2023. [Online]. Available: https://www.rand.org/pubs/conf_proceedings/CF380z1.html

[5] K. A. Edwards *et al.*, "Neuronally-derived tau is increased in experienced breachers and is associated with neurobehavioral symptoms," *Sci. Rep.*, vol. 11, p. 19527, Sep. 2021, doi: 10.1038/s41598-021-97913-0.

[6] S. Mallonee, S. Shariat, G. Stennies, R. Waxweiler, D. Hogan, and F. Jordan, "Physical Injuries and Fatalities Resulting From the Oklahoma City Bombing," *JAMA*, vol. 276, no. 5, pp. 382–387, Aug. 1996, doi: 10.1001/jama.1996.03540050042021.

[7] J. P. G. de Ceballos, F. Turégano-Fuentes, D. Perez-Diaz, M. Sanz-Sanchez, C. Martin-Llorente, and J. Guerrero-Sanz, "11 March 2004: The terrorist bomb explosions in Madrid, Spain – an analysis of the logistics, injuries sustained and clinical management of casualties treated at the closest hospital," *Crit. Care*, vol. 9, no. 1, pp. 104–111, 2005, doi: 10.1186/cc2995.

[8] A. K. Singh *et al.*, "Blast Injuries: From Improvised Explosive Device Blasts to the Boston Marathon Bombing," *RadioGraphics*, vol. 36, no. 1, pp. 295–307, Jan. 2016, doi: 10.1148/rg.2016150114.

[9] "Global Terrorism Database 1970 - 2020." START (National Consortium for the Study of Terrorism and Responses to Terrorism), 2022. Accessed: Apr. 12, 2023. [Online]. Available: https://www.start.umd.edu/gtd

[10] G. England, "Department of Defense Directive (DoDD) 6025.21E." United States Department of Defense, Jul. 05, 2006. Accessed: Mar. 28, 2023. [Online]. Available: https://www.esd.whs.mil/Portals/54/Documents/DD/issuances/dodd/602521p.pdf?ver=2018-10-24-112151-983

[11] H. R. Champion, J. B. Holcomb, and L. A. Young, "Injuries From Explosions: Physics, Biophysics, Pathology, and Required Research Focus," *J. Trauma Acute Care Surg.*, vol. 66, no. 5, p. 1468, May 2009, doi: 10.1097/TA.0b013e3181a27e7f.

[12] H. Phipps *et al.*, "Characteristics and Impact of U.S. Military Blast-Related Mild Traumatic Brain Injury: A Systematic Review," *Front. Neurol.*, vol. 11, 2020, Accessed: Apr. 07, 2023. [Online]. Available: https://www.frontiersin.org/articles/10.3389/fneur.2020.559318

[13] *Blast Injury Modalities*. Accessed: Apr. 01, 2023. [Online]. Available: https://stopcte.org/whats-cte/what-causes-cte/

[14] T. E. Scott, E. Kirkman, M. Haque, I. E. Gibb, P. Mahoney, and J. G. Hardman, “Primary blast lung injury - a review,” *Br. J. Anaesth.*, vol. 118, no. 3, pp. 311–316, Mar. 2017, doi: 10.1093/bja/aew385.

[15] S. J. Wolf, V. S. Bebarta, C. J. Bonnett, P. T. Pons, and S. V. Cantrill, “Blast injuries,” *The Lancet*, vol. 374, no. 9687, pp. 405–415, Aug. 2009, doi: 10.1016/S0140-6736(09)60257-9.

[16] F. Guilhaume-Correa, A. M. Pickrell, and P. J. VandeVord, “The Imbalance of Astrocytic Mitochondrial Dynamics Following Blast-Induced Traumatic Brain Injury,” *Biomedicines*, vol. 11, no. 2, Art. no. 2, Feb. 2023, doi: 10.3390/biomedicines11020329.

[17] H. J. Cho, V. S. S. S. Sajja, P. J. VandeVord, and Y. W. Lee, “Blast induces oxidative stress, inflammation, neuronal loss and subsequent short-term memory impairment in rats,” *Neuroscience*, vol. 253, pp. 9–20, Dec. 2013, doi: 10.1016/j.neuroscience.2013.08.037.

[18] N. Hlavac, “Attributes of Astrocyte Response to Mechano-Stimulation by High-Rate Overpressure,” Nov. 2018, Accessed: Dec. 12, 2022. [Online]. Available: https://vtechworks.lib.vt.edu/handle/10919/98534

[19] D. M. Adamson *et al.*, “Invisible Wounds of War: Psychological and Cognitive Injuries, Their Consequences, and Services to Assist Recovery,” RAND Corporation, Mar. 2008. Accessed: Apr. 07, 2023. [Online]. Available: https://www.rand.org/pubs/monographs/MG720.html

[20] H. M. Bramlett and W. D. Dietrich, “Long-Term Consequences of Traumatic Brain Injury: Current Status of Potential Mechanisms of Injury and Neurological Outcomes,” *J. Neurotrauma*, vol. 32, no. 23, pp. 1834–1848, Dec. 2015, doi: 10.1089/neu.2014.3352.

[21] J. W. Denny, R. J. Brown, M. G. Head, J. Batchelor, and A. S. Dickinson, “Allocation of funding into blast injury-related research and blast traumatic brain injury between 2000 and 2019: analysis of

global investments from public and philanthropic funders," *BMJ Mil Health*, vol. 169, no. 2, pp. 127–132, Apr. 2023, doi: 10.1136/bmjmilitary-2020-001655.

[22] D. V. Ritzel and S. Parks, "Shock Tube Apparatus for Blast Wave Simulation," US20130042665A1, Feb. 21, 2013 Accessed: Mar. 24, 2023. [Online]. Available: https://patents.google.com/patent/US20130042665A1/en

[23] A. Sundaramurthy *et al.*, "A 3-D Finite-Element Minipig Model to Assess Brain Biomechanical Responses to Blast Exposure," *Front. Bioeng. Biotechnol.*, vol. 9, 2021, Accessed: Apr. 07, 2023. [Online]. Available: https://www.frontiersin.org/articles/10.3389/fbioe.2021.757755

[24] A. S. Iwaskiw *et al.*, "The measurement of intracranial pressure and brain displacement due to short-duration dynamic overpressure loading," *Shock Waves*, vol. 28, no. 1, pp. 63–83, Jan. 2018, doi: 10.1007/s00193-017-0759-z.

[25] E. S. Bergmann-Leitner *et al.*, "Blast Waves Cause Immune System Dysfunction and Transient Bone Marrow Failure in a Mouse Model," *Front. Bioeng. Biotechnol.*, vol. 10, 2022, Accessed: Apr. 07, 2023. [Online]. Available: https://www.frontiersin.org/articles/10.3389/fbioe.2022.821169

[26] C. E. Hampton, C. N. Thorpe, C. A. Sholar, B. A. Rzigalinski, and P. J. VandeVord, "A novel bridge wire model of blast traumatic brain injury - biomed 2013," *Biomed. Sci. Instrum.*, vol. 49, pp. 312–319, 2013.

[27] J. Mediavilla Varas *et al.*, "Physics of IED Blast Shock Tube Simulations for mTBI Research," *Front. Neurol.*, vol. 2, 2011, Accessed: Dec. 12, 2022. [Online]. Available: https://www.frontiersin.org/articles/10.3389/fneur.2011.00058

[28] B. Rutter *et al.*, "Shock Wave Physics as Related to Primary Non-Impact Blast-Induced Traumatic Brain Injury," *Mil. Med.*, vol. 186, no. Supplement_1, pp. 601–609, Jan. 2021, doi: 10.1093/milmed/usaa290.

[29] I. G. Bowen, E. R. Fletcher, and D. R. Richmond, “ESTIMATE OF MAN’S TOLERANCE TO THE DIRECT EFFECTS OF AIR BLAST,” Oct. 1968. Accessed: Apr. 11, 2023. [Online]. Available: https://apps.dtic.mil/sti/citations/AD0693105

[30] E. Gruss, “A Correction for Primary Blast Injury Criteria,” *J. Trauma Acute Care Surg.*, vol. 60, no. 6, p. 1284, Jun. 2006, doi: 10.1097/01.ta.0000220015.21948.ec.

[31] P. A. Taylor, J. S. Ludwigsen, and C. C. Ford, “Investigation of blast-induced traumatic brain injury,” *Brain Inj.*, vol. 28, no. 7, pp. 879–895, Jun. 2014, doi: 10.3109/02699052.2014.888478.

[32] B. Rutter, “Pressure versus impulse graph for blast-induced traumatic brain injury and correlation to observable blast injuries,” *Dr. Diss.*, Jan. 2019, [Online]. Available: https://scholarsmine.mst.edu/doctoral_dissertations/2791

[33] M. Skotak, C. LaValle, A. Misistia, M. J. Egnoto, N. Chandra, and G. Kamimori, “Occupational Blast Wave Exposure During Multiday 0.50 Caliber Rifle Course,” *Front. Neurol.*, vol. 10, 2019, Accessed: May 08, 2023. [Online]. Available: https://www.frontiersin.org/articles/10.3389/fneur.2019.00797

[34] R. Han *et al.*, “Characteristics of exploding metal wires in water with three discharge types,” *J. Appl. Phys.*, vol. 122, no. 3, p. 033302, Jul. 2017, doi: 10.1063/1.4994009.

[35] X. Li, Y. Chao, J. Wu, R. Han, H. Zhou, and A. Qiu, “Study of the shock waves characteristics generated by underwater electrical wire explosion,” *J. Appl. Phys.*, vol. 118, no. 2, p. 023301, Jul. 2015, doi: 10.1063/1.4926374.

[36] R. Han *et al.*, “Experiments on the characteristics of underwater electrical wire explosions for reservoir stimulation,” *Matter Radiat. Extrem.*, vol. 5, no. 4, p. 047201, Jul. 2020, doi: 10.1063/1.5135725.

[37] S. Tanaka, D. Inao, K. Hasegawa, K. Hokamoto, P. Chen, and X. Gao, “Graphene Formation through Pulsed Wire Discharge of Graphite Strips in Water: Exfoliation Mechanism,” *Nanomaterials*, vol. 11, no. 5, Art. no. 5, May 2021, doi: 10.3390/nano11051223.

[38] Y. Fan, D. V. Mehta, I. M. Basheer, and A. J. MacIntosh, “A review on underwater shockwave processing and its application in food technology,” *Crit. Rev. Food Sci. Nutr.*, vol. 62, no. 4, pp. 980–988, Feb. 2022, doi: 10.1080/10408398.2020.1832439.

[39] Y. E. Krasik *et al.*, “Underwater Electrical Wire Explosion and Its Applications,” *IEEE Trans. Plasma Sci.*, vol. 36, no. 2, pp. 423–434, Apr. 2008, doi: 10.1109/TPS.2008.918766.

[40] W. Yao *et al.*, “An empirical approach for parameters estimation of underwater electrical wire explosion,” *Phys. Plasmas*, vol. 26, no. 9, p. 093502, Sep. 2019, doi: 10.1063/1.5111518.

[41] R. Han *et al.*, “A platform for exploding wires in different media,” *Rev. Sci. Instrum.*, vol. 88, no. 10, p. 103504, Oct. 2017, doi: 10.1063/1.4996027.

[42] L. Li, D. Qian, X. Zou, and X. Wang, “Effect of Deposition Energy on Underwater Electrical Wire Explosion,” *IEEE Trans. Plasma Sci.*, vol. 46, no. 10, pp. 3444–3449, Oct. 2018, doi: 10.1109/TPS.2018.2811124.

[43] B. Liu, D. Wang, and Y. Guo, “Effect of Circuit Parameters and Environment on Shock Waves Generated by Underwater Electrical Wire Explosion,” *IEEE Trans. Plasma Sci.*, vol. 45, no. 9, pp. 2519–2526, Sep. 2017, doi: 10.1109/TPS.2017.2739757.

[44] L. Li, D. Qian, Z. Liu, X. Zou, and X. Wang, “Comparison of underwater electrical wire explosions with large and small capacitors charged to a same energy,” *Phys. Plasmas*, vol. 27, no. 6, p. 063504 (9 pp.), Jun. 2020, doi: 10.1063/5.0005830.

[45] P. R. Berning and M. J. Coppinger, “An Exploding-Wire Circuit Model,” Jun. 2020.

[46] Y. E. Krasik *et al.*, “Underwater electrical wire explosion,” *Plasma Sources Sci. Technol.*, vol. 19, no. 3, p. 034020, May 2010, doi: 10.1088/0963-0252/19/3/034020.

[47] R. Han, H. Zhou, J. Wu, A. Qiu, W. Ding, and Y. Zhang, “Relationship between energy deposition and shock wave phenomenon in an underwater electrical wire explosion,” *Phys. Plasmas*, vol. 24, no. 9, p. 093506, Sep. 2017, doi: 10.1063/1.4989790.

[48] V. M. Romanova, G. V. Ivanenkov, A. R. Mingaleev, A. E. Ter-Oganesyan, T. A. Shelkovenko, and S. A. Pikuz, “Electric explosion of fine wires: Three groups of materials,” *Plasma Phys. Rep.*, vol. 41, no. 8, pp. 617–636, Aug. 2015, doi: 10.1134/S1063780X15080085.

[49] K.-J. Chung, K. Lee, Y. S. Hwang, and D.-K. Kim, “Numerical model for electrical explosion of copper wires in water,” *J. Appl. Phys.*, vol. 120, no. 20, p. 203301, Nov. 2016, doi: 10.1063/1.4968396.

[50] R. Bolander, B. Mathie, C. Bir, D. Ritzel, and P. VandeVord, “Skull Flexure as a Contributing Factor in the Mechanism of Injury in the Rat when Exposed to a Shock Wave,” *Ann. Biomed. Eng.*, vol. 39, no. 10, pp. 2550–2559, Oct. 2011, doi: 10.1007/s10439-011-0343-0.

[51] A. D. C. Leonardi, C. A. Bir, D. V. Ritzel, and P. J. VandeVord, “Intracranial Pressure Increases during Exposure to a Shock Wave,” *J. Neurotrauma*, vol. 28, no. 1, pp. 85–94, Jan. 2011, doi: 10.1089/neu.2010.1324.

[52] H. Song *et al.*, “Linking blast physics to biological outcomes in mild traumatic brain injury: Narrative review and preliminary report of an open-field blast model,” *Behav. Brain Res.*, vol. 340, pp. 147–158, Mar. 2018, doi: 10.1016/j.bbr.2016.08.037.

[53] C. E. Needham, D. Ritzel, G. T. Rule, S. Wiri, and L. Young, “Blast Testing Issues and TBI: Experimental Models That Lead to Wrong Conclusions,” *Front. Neurol.*, vol. 6, 2015, Accessed: Mar. 30, 2023. [Online]. Available: https://www.frontiersin.org/articles/10.3389/fneur.2015.00072

APPENDIX A: TUKEY-KRAMER HSD PAIRED MEANS COMPARISON

A.1 TUKEY-KRAMER PAIRS FOR PEAK OVERPRESSURE

A.1.1 Pairs of Wire Materials

Level	- Level	Difference	Std Err Dif	Lower CL	Upper CL	p-Value
Cu	SS	3.273841	1.368347	-0.57458	7.122263	0.1315
NiCr	SS	3.104276	1.368347	-0.74415	6.952699	0.1695
Cu	W	2.294046	1.368347	-1.55438	6.142468	0.4560
NiCr	W	2.124481	1.368347	-1.72394	5.972903	0.5331
Ag	SS	1.961058	1.368347	-1.88736	5.809481	0.6091
Cu	Ag	1.312783	1.368347	-2.53564	5.161205	0.8721
NiCr	Ag	1.143218	1.368347	-2.70520	4.991640	0.9185
Ag	W	0.981263	1.368347	-2.86716	4.829685	0.9518
W	SS	0.979795	1.368347	-2.86863	4.828218	0.9520
Cu	NiCr	0.169565	1.368347	-3.67886	4.017987	0.9999

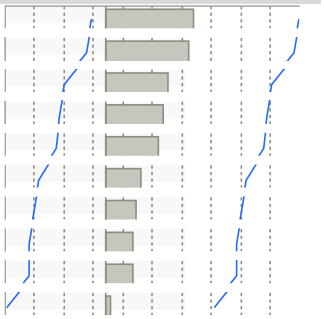

A.1.2 Pairs of Wire Diameters

Level	- Level	Difference	Std Err Dif	Lower CL	Upper CL	p-Value
36	32	13.91380	1.059917	11.3666	16.46102	<.0001*
40	32	11.60681	1.059917	9.0596	14.15403	<.0001*
36	40	2.30699	1.059917	-0.2402	4.85421	0.0835

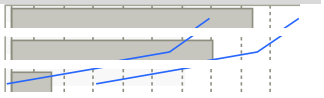

A.1.3 Pairs of Combinations of Wire Material and Diameter

Level	- Level	Difference	Std Err Dif	Lower CL	Upper CL	p-Value
Cu,36	SS,32	20.31329	2.370047	11.9320	28.69454	<.0001*
Cu,36	W,32	19.74763	2.370047	11.3664	28.12888	<.0001*
Cu,36	Ag,32	19.48625	2.370047	11.1050	27.86750	<.0001*
Cu,36	NiCr,32	18.75364	2.370047	10.3724	27.13489	<.0001*
Cu,36	Cu,32	17.83019	2.370047	9.4489	26.21144	<.0001*
Ag,36	SS,32	16.48749	2.370047	8.1062	24.86875	<.0001*
Ag,36	W,32	15.92183	2.370047	7.5406	24.30308	<.0001*
Ag,36	Ag,32	15.66046	2.370047	7.2792	24.04171	<.0001*
NiCr,36	SS,32	15.51742	2.370047	7.1362	23.89867	<.0001*
NiCr,40	SS,32	15.42626	2.370047	7.0450	23.80751	<.0001*
NiCr,36	W,32	14.95176	2.370047	6.5705	23.33301	<.0001*
Ag,36	NiCr,32	14.92785	2.370047	6.5466	23.30910	<.0001*
W,40	SS,32	14.92154	2.370047	6.5403	23.30279	<.0001*
NiCr,40	W,32	14.86060	2.370047	6.4793	23.24185	<.0001*
NiCr,36	Ag,32	14.69038	2.370047	6.3091	23.07163	<.0001*
NiCr,40	Ag,32	14.59922	2.370047	6.2180	22.98047	<.0001*
W,40	W,32	14.35588	2.370047	5.9746	22.73713	<.0001*

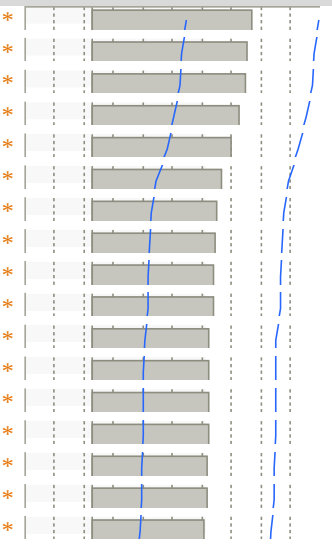

Level	- Level	Difference	Std Err Dif	Lower CL	Upper CL	p-Value
W,40	Ag,32	14.09450	2.370047	5.7132	22.47575	<.0001*
Ag,36	Cu,32	14.00440	2.370047	5.6231	22.38565	<.0001*
NiCr,36	NiCr,32	13.95777	2.370047	5.5765	22.33902	<.0001*
NiCr,40	NiCr,32	13.86661	2.370047	5.4854	22.24786	<.0001*
W,40	NiCr,32	13.36189	2.370047	4.9806	21.74314	<.0001*
NiCr,36	Cu,32	13.03432	2.370047	4.6531	21.41557	<.0001*
NiCr,40	Cu,32	12.94316	2.370047	4.5619	21.32441	<.0001*
W,40	Cu,32	12.43844	2.370047	4.0572	20.81969	0.0002*
SS,36	SS,32	12.04357	2.370047	3.6623	20.42482	0.0004*
Ag,40	SS,32	11.75914	2.370047	3.3779	20.14039	0.0005*
SS,36	W,32	11.47790	2.370047	3.0967	19.85916	0.0008*
SS,36	Ag,32	11.21653	2.370047	2.8353	19.59778	0.0012*
Ag,40	W,32	11.19348	2.370047	2.8122	19.57473	0.0013*
SS,40	SS,32	11.14693	2.370047	2.7657	19.52818	0.0013*
Ag,40	Ag,32	10.93210	2.370047	2.5508	19.31335	0.0018*
W,36	SS,32	10.64269	2.370047	2.2614	19.02394	0.0028*
SS,40	W,32	10.58127	2.370047	2.2000	18.96252	0.0030*
SS,36	NiCr,32	10.48392	2.370047	2.1027	18.86517	0.0034*
SS,40	Ag,32	10.31989	2.370047	1.9386	18.70114	0.0043*
Cu,40	SS,32	10.21564	2.370047	1.8344	18.59689	0.0050*
Ag,40	NiCr,32	10.19949	2.370047	1.8182	18.58074	0.0051*
Cu,36	Cu,40	10.09765	2.370047	1.7164	18.47890	0.0058*
W,36	W,32	10.07703	2.370047	1.6958	18.45828	0.0060*
W,36	Ag,32	9.81565	2.370047	1.4344	18.19690	0.0085*
Cu,36	W,36	9.67060	2.370047	1.2894	18.05185	0.0103*
Cu,40	W,32	9.64997	2.370047	1.2687	18.03123	0.0106*
SS,40	NiCr,32	9.58728	2.370047	1.2060	17.96853	0.0115*
SS,36	Cu,32	9.56047	2.370047	1.1792	17.94172	0.0119*
Cu,40	Ag,32	9.38860	2.370047	1.0073	17.76985	0.0148*
Ag,40	Cu,32	9.27604	2.370047	0.8948	17.65729	0.0171*
Cu,36	SS,40	9.16635	2.370047	0.7851	17.54760	0.0196*
W,36	NiCr,32	9.08304	2.370047	0.7018	17.46429	0.0218*
SS,40	Cu,32	8.66383	2.370047	0.2826	17.04508	0.0361*
Cu,40	NiCr,32	8.65599	2.370047	0.2747	17.03724	0.0364*
Cu,36	Ag,40	8.55415	2.370047	0.1729	16.93540	0.0410*
Cu,36	SS,36	8.26972	2.370047	-0.1115	16.65097	0.0567
W,36	Cu,32	8.15959	2.370047	-0.2217	16.54084	0.0640
Cu,40	Cu,32	7.73254	2.370047	-0.6487	16.11379	0.1008
Ag,36	Cu,40	6.27186	2.370047	-2.1094	14.65311	0.3619
Ag,36	W,36	5.84481	2.370047	-2.5364	14.22606	0.4790
Cu,36	W,40	5.39175	2.370047	-2.9895	13.77300	0.6119
Ag,36	SS,40	5.34056	2.370047	-3.0407	13.72181	0.6269
NiCr,36	Cu,40	5.30178	2.370047	-3.0795	13.68303	0.6382
NiCr,40	Cu,40	5.21062	2.370047	-3.1706	13.59187	0.6645
Cu,36	NiCr,40	4.88703	2.370047	-3.4942	13.26828	0.7533
NiCr,36	W,36	4.87473	2.370047	-3.5065	13.25598	0.7565
Cu,36	NiCr,36	4.79587	2.370047	-3.5854	13.17712	0.7765
NiCr,40	W,36	4.78357	2.370047	-3.5977	13.16482	0.7795
Ag,36	Ag,40	4.72836	2.370047	-3.6529	13.10961	0.7930
W,40	Cu,40	4.70590	2.370047	-3.6753	13.08715	0.7984
Ag,36	SS,36	4.44393	2.370047	-3.9373	12.82518	0.8558
NiCr,36	SS,40	4.37049	2.370047	-4.0108	12.75174	0.8700
NiCr,40	SS,40	4.27933	2.370047	-4.1019	12.66058	0.8865

Level	- Level	Difference	Std Err Dif	Lower CL	Upper CL	p-Value
W,40	W,36	4.27885	2.370047	-4.1024	12.66010	0.8866
Cu,36	Ag,36	3.82579	2.370047	-4.5555	12.20704	0.9487
W,40	SS,40	3.77461	2.370047	-4.6066	12.15586	0.9538
NiCr,36	Ag,40	3.75828	2.370047	-4.6230	12.13953	0.9553
NiCr,40	Ag,40	3.66712	2.370047	-4.7141	12.04837	0.9632
NiCr,36	SS,36	3.47385	2.370047	-4.9074	11.85510	0.9765
NiCr,40	SS,36	3.38269	2.370047	-4.9986	11.76394	0.9813
W,40	Ag,40	3.16240	2.370047	-5.2189	11.54365	0.9898
W,40	SS,36	2.87797	2.370047	-5.5033	11.25922	0.9959
Cu,32	SS,32	2.48310	2.370047	-5.8982	10.86435	0.9991
Cu,32	W,32	1.91744	2.370047	-6.4638	10.29869	1.0000
SS,36	Cu,40	1.82793	2.370047	-6.5533	10.20918	1.0000
Cu,32	Ag,32	1.65606	2.370047	-6.7252	10.03731	1.0000
Ag,36	W,40	1.56596	2.370047	-6.8153	9.94721	1.0000
NiCr,32	SS,32	1.55965	2.370047	-6.8216	9.94090	1.0000
Ag,40	Cu,40	1.54350	2.370047	-6.8377	9.92475	1.0000
SS,36	W,36	1.40088	2.370047	-6.9804	9.78213	1.0000
Ag,40	W,36	1.11645	2.370047	-7.2648	9.49770	1.0000
Ag,36	NiCr,40	1.06124	2.370047	-7.3200	9.44249	1.0000
NiCr,32	W,32	0.99399	2.370047	-7.3873	9.37524	1.0000
Ag,36	NiCr,36	0.97008	2.370047	-7.4112	9.35133	1.0000
SS,40	Cu,40	0.93130	2.370047	-7.4500	9.31255	1.0000
Cu,32	NiCr,32	0.92345	2.370047	-7.4578	9.30470	1.0000
SS,36	SS,40	0.89663	2.370047	-7.4846	9.27788	1.0000
Ag,32	SS,32	0.82704	2.370047	-7.5542	9.20829	1.0000
NiCr,32	Ag,32	0.73261	2.370047	-7.6486	9.11386	1.0000
Ag,40	SS,40	0.61221	2.370047	-7.7690	8.99346	1.0000
NiCr,36	W,40	0.59588	2.370047	-7.7854	8.97713	1.0000
W,32	SS,32	0.56566	2.370047	-7.8156	8.94691	1.0000
NiCr,40	W,40	0.50472	2.370047	-7.8765	8.88597	1.0000
SS,40	W,36	0.50425	2.370047	-7.8770	8.88550	1.0000
W,36	Cu,40	0.42705	2.370047	-7.9542	8.80830	1.0000
SS,36	Ag,40	0.28443	2.370047	-8.0968	8.66568	1.0000
Ag,32	W,32	0.26138	2.370047	-8.1199	8.64263	1.0000
NiCr,36	NiCr,40	0.09116	2.370047	-8.2901	8.47241	1.0000

A.2 Positive Duration

A.2.1 Pairs of Wire Materials

Level	- Level	Difference	Std Err Dif	Lower CL	Upper CL	p-Value
NiCr	Ag	0.1204000	0.0376272	0.014575	0.2262251	0.0180*
NiCr	W	0.1200667	0.0376272	0.014242	0.2258918	0.0185*
SS	Ag	0.0856667	0.0376272	-0.020158	0.1914918	0.1668
SS	W	0.0853333	0.0376272	-0.020492	0.1911584	0.1698
NiCr	Cu	0.0714667	0.0376272	-0.034358	0.1772918	0.3289
Cu	Ag	0.0489333	0.0376272	-0.056892	0.1547584	0.6919
Cu	W	0.0486000	0.0376272	-0.057225	0.1544251	0.6973
SS	Cu	0.0367333	0.0376272	-0.069092	0.1425584	0.8648
NiCr	SS	0.0347333	0.0376272	-0.071092	0.1405584	0.8869

Level	- Level	Difference	Std Err Dif	Lower CL	Upper CL	p-Value
W	Ag	0.0003333	0.0376272	-0.105492	0.1061584	1.0000

A.2.2 Pairs of Wire Diameters

Level	- Level	Difference	Std Err Dif	Lower CL	Upper CL	p-Value
36	32	0.1605600	0.0291459	0.090516	0.2306042	<.0001*
40	32	0.1037600	0.0291459	0.033716	0.1738042	0.0021*
36	40	0.0568000	0.0291459	-0.013244	0.1268442	0.1340

A.2.3 Pairs of Combinations of Wire Material and Diameter

Level	- Level	Difference	Std Err Dif	Lower CL	Upper CL	p-Value
Ag,36	Ag,40	0.3254000	0.0651723	0.094930	0.5558702	0.0005*
SS,40	Ag,40	0.3252000	0.0651723	0.094730	0.5556702	0.0005*
Cu,36	Ag,40	0.3072000	0.0651723	0.076730	0.5376702	0.0013*
Ag,36	Cu,32	0.2968000	0.0651723	0.066330	0.5272702	0.0022*
SS,40	Cu,32	0.2966000	0.0651723	0.066130	0.5270702	0.0023*
Ag,36	W,32	0.2926000	0.0651723	0.062130	0.5230702	0.0028*
SS,40	W,32	0.2924000	0.0651723	0.061930	0.5228702	0.0028*
Cu,36	Cu,32	0.2786000	0.0651723	0.048130	0.5090702	0.0056*
Cu,36	W,32	0.2744000	0.0651723	0.043930	0.5048702	0.0069*
NiCr,32	Ag,40	0.2742000	0.0651723	0.043730	0.5046702	0.0069*
NiCr,40	Ag,40	0.2714000	0.0651723	0.040930	0.5018702	0.0079*
SS,36	Ag,40	0.2672000	0.0651723	0.036730	0.4976702	0.0097*
NiCr,32	Cu,32	0.2456000	0.0651723	0.015130	0.4760702	0.0262*
NiCr,40	Cu,32	0.2428000	0.0651723	0.012330	0.4732702	0.0296*
NiCr,32	W,32	0.2414000	0.0651723	0.010930	0.4718702	0.0315*
Ag,36	SS,32	0.2408000	0.0651723	0.010330	0.4712702	0.0323*
SS,40	SS,32	0.2406000	0.0651723	0.010130	0.4710702	0.0326*
SS,36	Cu,32	0.2386000	0.0651723	0.008130	0.4690702	0.0355*
NiCr,40	W,32	0.2386000	0.0651723	0.008130	0.4690702	0.0355*
NiCr,36	Ag,40	0.2356000	0.0651723	0.005130	0.4660702	0.0404*
SS,36	W,32	0.2344000	0.0651723	0.003930	0.4648702	0.0425*
Cu,40	Ag,40	0.2310000	0.0651723	0.000530	0.4614702	0.0489*
Ag,36	Ag,32	0.2308000	0.0651723	0.000330	0.4612702	0.0493*
SS,40	Ag,32	0.2306000	0.0651723	0.000130	0.4610702	0.0497*
Cu,36	SS,32	0.2226000	0.0651723	-0.007870	0.4530702	0.0687
Cu,36	Ag,32	0.2126000	0.0651723	-0.017870	0.4430702	0.1009
NiCr,36	Cu,32	0.2070000	0.0651723	-0.023470	0.4374702	0.1238
W,40	Ag,40	0.2060000	0.0651723	-0.024470	0.4364702	0.1283
NiCr,36	W,32	0.2028000	0.0651723	-0.027670	0.4332702	0.1436
Cu,40	Cu,32	0.2024000	0.0651723	-0.028070	0.4328702	0.1456
Cu,40	W,32	0.1982000	0.0651723	-0.032270	0.4286702	0.1681
NiCr,32	SS,32	0.1896000	0.0651723	-0.040870	0.4200702	0.2220
NiCr,40	SS,32	0.1868000	0.0651723	-0.043670	0.4172702	0.2419
SS,36	SS,32	0.1826000	0.0651723	-0.047870	0.4130702	0.2740
W,36	Ag,40	0.1822000	0.0651723	-0.048270	0.4126702	0.2772
NiCr,32	Ag,32	0.1796000	0.0651723	-0.050870	0.4100702	0.2986
W,40	Cu,32	0.1774000	0.0651723	-0.053070	0.4078702	0.3174
NiCr,40	Ag,32	0.1768000	0.0651723	-0.053670	0.4072702	0.3226
W,40	W,32	0.1732000	0.0651723	-0.057270	0.4036702	0.3551
SS,36	Ag,32	0.1726000	0.0651723	-0.057870	0.4030702	0.3607
W,36	Cu,32	0.1536000	0.0651723	-0.076870	0.3840702	0.5547
NiCr,36	SS,32	0.1510000	0.0651723	-0.079470	0.3814702	0.5826
W,36	W,32	0.1494000	0.0651723	-0.081070	0.3798702	0.5998

Level	- Level	Difference	Std Err Dif	Lower CL	Upper CL	p-Value
Cu,40	SS,32	0.1464000	0.0651723	-0.084070	0.3768702	0.6318
Ag,36	W,36	0.1432000	0.0651723	-0.087270	0.3736702	0.6654
SS,40	W,36	0.1430000	0.0651723	-0.087470	0.3734702	0.6675
NiCr,36	Ag,32	0.1410000	0.0651723	-0.089470	0.3714702	0.6881
Cu,40	Ag,32	0.1364000	0.0651723	-0.094070	0.3668702	0.7340
Cu,36	W,36	0.1250000	0.0651723	-0.105470	0.3554702	0.8347
W,40	SS,32	0.1214000	0.0651723	-0.109070	0.3518702	0.8615
Ag,36	W,40	0.1194000	0.0651723	-0.111070	0.3498702	0.8753
SS,40	W,40	0.1192000	0.0651723	-0.111270	0.3496702	0.8766
W,40	Ag,32	0.1114000	0.0651723	-0.119070	0.3418702	0.9219
Cu,36	W,40	0.1012000	0.0651723	-0.129270	0.3316702	0.9622
W,36	SS,32	0.0976000	0.0651723	-0.132870	0.3280702	0.9718
Ag,32	Ag,40	0.0946000	0.0651723	-0.135870	0.3250702	0.9784
Ag,36	Cu,40	0.0944000	0.0651723	-0.136070	0.3248702	0.9788
SS,40	Cu,40	0.0942000	0.0651723	-0.136270	0.3246702	0.9791
NiCr,32	W,36	0.0920000	0.0651723	-0.138470	0.3224702	0.9830
Ag,36	NiCr,36	0.0898000	0.0651723	-0.140670	0.3202702	0.9863
SS,40	NiCr,36	0.0896000	0.0651723	-0.140870	0.3200702	0.9866
NiCr,40	W,36	0.0892000	0.0651723	-0.141270	0.3196702	0.9871
W,36	Ag,32	0.0876000	0.0651723	-0.142870	0.3180702	0.9891
SS,36	W,36	0.0850000	0.0651723	-0.145470	0.3154702	0.9918
SS,32	Ag,40	0.0846000	0.0651723	-0.145870	0.3150702	0.9921
Cu,36	Cu,40	0.0762000	0.0651723	-0.154270	0.3066702	0.9972
Cu,36	NiCr,36	0.0716000	0.0651723	-0.158870	0.3020702	0.9985
NiCr,32	W,40	0.0682000	0.0651723	-0.162270	0.2986702	0.9991
Ag,32	Cu,32	0.0660000	0.0651723	-0.164470	0.2964702	0.9994
NiCr,40	W,40	0.0654000	0.0651723	-0.165070	0.2958702	0.9994
Ag,32	W,32	0.0618000	0.0651723	-0.168670	0.2922702	0.9997
SS,36	W,40	0.0612000	0.0651723	-0.169270	0.2916702	0.9997
Ag,36	SS,36	0.0582000	0.0651723	-0.172270	0.2886702	0.9999
SS,40	SS,36	0.0580000	0.0651723	-0.172470	0.2884702	0.9999
SS,32	Cu,32	0.0560000	0.0651723	-0.174470	0.2864702	0.9999
Ag,36	NiCr,40	0.0540000	0.0651723	-0.176470	0.2844702	0.9999
SS,40	NiCr,40	0.0538000	0.0651723	-0.176670	0.2842702	0.9999
NiCr,36	W,36	0.0534000	0.0651723	-0.177070	0.2838702	0.9999
SS,32	W,32	0.0518000	0.0651723	-0.178670	0.2822702	1.0000
Ag,36	NiCr,32	0.0512000	0.0651723	-0.179270	0.2816702	1.0000
SS,40	NiCr,32	0.0510000	0.0651723	-0.179470	0.2814702	1.0000
Cu,40	W,36	0.0488000	0.0651723	-0.181670	0.2792702	1.0000
NiCr,32	Cu,40	0.0432000	0.0651723	-0.187270	0.2736702	1.0000
NiCr,40	Cu,40	0.0404000	0.0651723	-0.190070	0.2708702	1.0000
Cu,36	SS,36	0.0400000	0.0651723	-0.190470	0.2704702	1.0000
NiCr,32	NiCr,36	0.0386000	0.0651723	-0.191870	0.2690702	1.0000
SS,36	Cu,40	0.0362000	0.0651723	-0.194270	0.2666702	1.0000
Cu,36	NiCr,40	0.0358000	0.0651723	-0.194670	0.2662702	1.0000
NiCr,40	NiCr,36	0.0358000	0.0651723	-0.194670	0.2662702	1.0000
Cu,36	NiCr,32	0.0330000	0.0651723	-0.197470	0.2634702	1.0000
W,32	Ag,40	0.0328000	0.0651723	-0.197670	0.2632702	1.0000
SS,36	NiCr,36	0.0316000	0.0651723	-0.198870	0.2620702	1.0000
NiCr,36	W,40	0.0296000	0.0651723	-0.200870	0.2600702	1.0000
Cu,32	Ag,40	0.0286000	0.0651723	-0.201870	0.2590702	1.0000
Cu,40	W,40	0.0250000	0.0651723	-0.205470	0.2554702	1.0000
W,40	W,36	0.0238000	0.0651723	-0.206670	0.2542702	1.0000
Ag,36	Cu,36	0.0182000	0.0651723	-0.212270	0.2486702	1.0000
SS,40	Cu,36	0.0180000	0.0651723	-0.212470	0.2484702	1.0000
Ag,32	SS,32	0.0100000	0.0651723	-0.220470	0.2404702	1.0000
NiCr,32	SS,36	0.0070000	0.0651723	-0.223470	0.2374702	1.0000
NiCr,36	Cu,40	0.0046000	0.0651723	-0.225870	0.2350702	1.0000
W,32	Cu,32	0.0042000	0.0651723	-0.226270	0.2346702	1.0000
NiCr,40	SS,36	0.0042000	0.0651723	-0.226270	0.2346702	1.0000
NiCr,32	NiCr,40	0.0028000	0.0651723	-0.227670	0.2332702	1.0000

Level	- Level	Difference	Std Err Dif	Lower CL	Upper CL	p-Value
Ag,36	SS,40	0.0002000	0.0651723	-0.230270	0.2306702	1.0000

A.3 Positive Impulse

A.3.1 Pairs of Wire Material

Level	- Level	Difference	Std Err Dif	Lower CL	Upper CL	p-Value
NiCr	Ag	1.010135	0.1501338	0.587889	1.432380	<.0001*
NiCr	SS	0.800175	0.1501338	0.377930	1.222420	<.0001*
W	Ag	0.711526	0.1501338	0.289280	1.133771	0.0001*
Cu	Ag	0.646261	0.1501338	0.224016	1.068507	0.0006*
W	SS	0.501566	0.1501338	0.079321	0.923811	0.0121*
Cu	SS	0.436302	0.1501338	0.014056	0.858547	0.0395*
NiCr	Cu	0.363873	0.1501338	-0.058372	0.786119	0.1231
NiCr	W	0.298609	0.1501338	-0.123636	0.720854	0.2838
SS	Ag	0.209960	0.1501338	-0.212286	0.632205	0.6310
W	Cu	0.065264	0.1501338	-0.356981	0.487509	0.9924

A.3.2 Pairs of Wire Diameters

Level	- Level	Difference	Std Err Dif	Lower CL	Upper CL	p-Value
36	32	4.873208	0.1162931	4.593730	5.152687	<.0001*
40	32	4.375825	0.1162931	4.096346	4.655303	<.0001*
36	40	0.497384	0.1162931	0.217905	0.776862	0.0002*

A.3.3 Pairs of Combinations of Wire Material and Diameter

Level	- Level	Difference	Std Err Dif	Lower CL	Upper CL	p-Value
NiCr,40	SS,32	6.438669	0.2600393	5.51909	7.358252	<.0001*
NiCr,40	W,32	6.315543	0.2600393	5.39596	7.235126	<.0001*
Cu,36	SS,32	6.070757	0.2600393	5.15117	6.990340	<.0001*
NiCr,40	Ag,32	6.057760	0.2600393	5.13818	6.977343	<.0001*
W,40	SS,32	5.985826	0.2600393	5.06624	6.905408	<.0001*
Cu,36	W,32	5.947631	0.2600393	5.02805	6.867214	<.0001*
Ag,36	SS,32	5.937943	0.2600393	5.01836	6.857526	<.0001*
W,40	W,32	5.862699	0.2600393	4.94312	6.782282	<.0001*
Ag,36	W,32	5.814816	0.2600393	4.89523	6.734399	<.0001*
Cu,36	Ag,32	5.689848	0.2600393	4.77026	6.609430	<.0001*
NiCr,40	NiCr,32	5.685891	0.2600393	4.76631	6.605473	<.0001*
W,40	Ag,32	5.604916	0.2600393	4.68533	6.524499	<.0001*
Ag,36	Ag,32	5.557033	0.2600393	4.63745	6.476616	<.0001*
NiCr,40	Cu,32	5.539604	0.2600393	4.62002	6.459187	<.0001*
Cu,36	NiCr,32	5.317978	0.2600393	4.39840	6.237561	<.0001*
W,40	NiCr,32	5.233047	0.2600393	4.31346	6.152630	<.0001*
Ag,36	NiCr,32	5.185164	0.2600393	4.26558	6.104747	<.0001*
Cu,36	Cu,32	5.171692	0.2600393	4.25211	6.091275	<.0001*
W,40	Cu,32	5.086760	0.2600393	4.16718	6.006343	<.0001*
Ag,36	Cu,32	5.038877	0.2600393	4.11929	5.958460	<.0001*

Level	- Level	Difference	Std Err Dif	Lower CL	Upper CL	p-Value
W,36	SS,32	5.021457	0.2600393	4.10187	5.941040	<.0001*
SS,40	SS,32	4.968735	0.2600393	4.04915	5.888318	<.0001*
W,36	W,32	4.898330	0.2600393	3.97875	5.817913	<.0001*
SS,40	W,32	4.845608	0.2600393	3.92603	5.765191	<.0001*
NiCr,36	SS,32	4.834788	0.2600393	3.91521	5.754371	<.0001*
NiCr,36	W,32	4.711662	0.2600393	3.79208	5.631245	<.0001*
SS,36	SS,32	4.656976	0.2600393	3.73739	5.576559	<.0001*
W,36	Ag,32	4.640547	0.2600393	3.72096	5.560130	<.0001*
SS,40	Ag,32	4.587825	0.2600393	3.66824	5.507408	<.0001*
SS,36	W,32	4.533850	0.2600393	3.61427	5.453433	<.0001*
NiCr,36	Ag,32	4.453879	0.2600393	3.53430	5.373462	<.0001*
SS,36	Ag,32	4.276067	0.2600393	3.35648	5.195650	<.0001*
W,36	NiCr,32	4.268678	0.2600393	3.34910	5.188261	<.0001*
SS,40	NiCr,32	4.215956	0.2600393	3.29637	5.135539	<.0001*
W,36	Cu,32	4.122392	0.2600393	3.20281	5.041974	<.0001*
NiCr,36	NiCr,32	4.082009	0.2600393	3.16243	5.001592	<.0001*
SS,40	Cu,32	4.069669	0.2600393	3.15009	4.989252	<.0001*
Cu,40	SS,32	3.964794	0.2600393	3.04521	4.884377	<.0001*
NiCr,36	Cu,32	3.935723	0.2600393	3.01614	4.855306	<.0001*
SS,36	NiCr,32	3.904198	0.2600393	2.98461	4.823780	<.0001*
Cu,40	W,32	3.841667	0.2600393	2.92208	4.761250	<.0001*
NiCr,40	Ag,40	3.761690	0.2600393	2.84211	4.681272	<.0001*
SS,36	Cu,32	3.757911	0.2600393	2.83833	4.677494	<.0001*
Cu,40	Ag,32	3.583884	0.2600393	2.66430	4.503467	<.0001*
Cu,36	Ag,40	3.393777	0.2600393	2.47419	4.313360	<.0001*
W,40	Ag,40	3.308846	0.2600393	2.38926	4.228429	<.0001*
Ag,36	Ag,40	3.260963	0.2600393	2.34138	4.180546	<.0001*
Cu,40	NiCr,32	3.212015	0.2600393	2.29243	4.131598	<.0001*
Cu,40	Cu,32	3.065728	0.2600393	2.14615	3.985311	<.0001*
Ag,40	SS,32	2.676980	0.2600393	1.75740	3.596563	<.0001*
Ag,40	W,32	2.553853	0.2600393	1.63427	3.473436	<.0001*
NiCr,40	Cu,40	2.473876	0.2600393	1.55429	3.393458	<.0001*
W,36	Ag,40	2.344477	0.2600393	1.42489	3.264060	<.0001*
Ag,40	Ag,32	2.296070	0.2600393	1.37649	3.215653	<.0001*
SS,40	Ag,40	2.291755	0.2600393	1.37217	3.211338	<.0001*
NiCr,36	Ag,40	2.157808	0.2600393	1.23823	3.077391	<.0001*
Cu,36	Cu,40	2.105963	0.2600393	1.18638	3.025546	<.0001*
W,40	Cu,40	2.021032	0.2600393	1.10145	2.940615	<.0001*
SS,36	Ag,40	1.979997	0.2600393	1.06041	2.899579	<.0001*
Ag,36	Cu,40	1.973149	0.2600393	1.05357	2.892732	<.0001*
Ag,40	NiCr,32	1.924201	0.2600393	1.00462	2.843784	<.0001*
NiCr,40	SS,36	1.781693	0.2600393	0.86211	2.701276	<.0001*
Ag,40	Cu,32	1.777914	0.2600393	0.85833	2.697497	<.0001*
NiCr,40	NiCr,36	1.603881	0.2600393	0.68430	2.523464	<.0001*
NiCr,40	SS,40	1.469935	0.2600393	0.55035	2.389518	<.0001*
NiCr,40	W,36	1.417212	0.2600393	0.49763	2.336795	<.0001*
Cu,36	SS,36	1.413781	0.2600393	0.49420	2.333364	<.0001*
W,40	SS,36	1.328849	0.2600393	0.40927	2.248432	0.0003*
Cu,40	Ag,40	1.287814	0.2600393	0.36823	2.207397	0.0006*
Ag,36	SS,36	1.280966	0.2600393	0.36138	2.200549	0.0006*
Cu,36	NiCr,36	1.235969	0.2600393	0.31639	2.155552	0.0011*
W,40	NiCr,36	1.151037	0.2600393	0.23145	2.070620	0.0034*
Ag,36	NiCr,36	1.103155	0.2600393	0.18357	2.022737	0.0062*
Cu,36	SS,40	1.102022	0.2600393	0.18244	2.021605	0.0063*
W,36	Cu,40	1.056663	0.2600393	0.13708	1.976246	0.0109*
Cu,36	W,36	1.049300	0.2600393	0.12972	1.968883	0.0119*
W,40	SS,40	1.017091	0.2600393	0.09751	1.936674	0.0172*
SS,40	Cu,40	1.003941	0.2600393	0.08436	1.923524	0.0200*
Ag,36	SS,40	0.969208	0.2600393	0.04963	1.888791	0.0295*
W,40	W,36	0.964369	0.2600393	0.04479	1.883952	0.0311*
Ag,36	W,36	0.916486	0.2600393	-0.00310	1.836069	0.0516

Level	- Level	Difference	Std Err Dif	Lower CL	Upper CL	p-Value
Cu,32	SS,32	0.899065	0.2600393	-0.02052	1.818648	0.0616
NiCr,36	Cu,40	0.869994	0.2600393	-0.04959	1.789577	0.0821
Cu,32	W,32	0.775939	0.2600393	-0.14364	1.695522	0.1901
NiCr,32	SS,32	0.752779	0.2600393	-0.16680	1.672362	0.2285
SS,36	Cu,40	0.692183	0.2600393	-0.22740	1.611766	0.3525
NiCr,32	W,32	0.629652	0.2600393	-0.28993	1.549235	0.5097
Cu,32	Ag,32	0.518156	0.2600393	-0.40143	1.437739	0.7944
NiCr,40	Ag,36	0.500727	0.2600393	-0.41886	1.420309	0.8308
NiCr,40	W,40	0.452844	0.2600393	-0.46674	1.372427	0.9110
Ag,32	SS,32	0.380910	0.2600393	-0.53867	1.300492	0.9766
NiCr,32	Ag,32	0.371869	0.2600393	-0.54771	1.291452	0.9810
NiCr,40	Cu,36	0.367912	0.2600393	-0.55167	1.287495	0.9827
W,36	SS,36	0.364480	0.2600393	-0.55510	1.284063	0.9841
SS,40	SS,36	0.311758	0.2600393	-0.60782	1.231341	0.9964
Ag,32	W,32	0.257783	0.2600393	-0.66180	1.177366	0.9995
W,36	NiCr,36	0.186669	0.2600393	-0.73291	1.106252	1.0000
NiCr,36	SS,36	0.177812	0.2600393	-0.74177	1.097395	1.0000
Cu,32	NiCr,32	0.146287	0.2600393	-0.77330	1.065869	1.0000
SS,40	NiCr,36	0.133946	0.2600393	-0.78564	1.053529	1.0000
Cu,36	Ag,36	0.132814	0.2600393	-0.78677	1.052397	1.0000
W,32	SS,32	0.123126	0.2600393	-0.79646	1.042709	1.0000
Cu,36	W,40	0.084932	0.2600393	-0.83465	1.004514	1.0000
W,36	SS,40	0.052722	0.2600393	-0.86686	0.972305	1.0000
W,40	Ag,36	0.047883	0.2600393	-0.87170	0.967466	1.0000